Pulmonary Infections: Imaging with CT

Catherine Beigelman-Aubry and Sabine Schmidt

Abstract

Computed tomography (CT) plays a key role in various kinds of pulmonary infections especially in immunocompromised patients, owing to its much higher sensitivity and specificity than the traditionally performed chest X-ray. CT permits the detection of the main infectious pattern and associated findings with high confidence and allows for the precise assessment of all involved structures, to potentially guide a bronchoalveolar lavage or another diagnostic procedure, and to ensure a reliable follow-up. It may be performed at a carefully chosen dose, which may nearly reach that of a chest X-ray in specific situations. The importance of post-processing tools is undeniable in some conditions, in particular for the evaluation of micronodules in the immunocompromised population. The wide spectrum of features of specific organisms according to the immune status, such as in aspergillosis or tuberculosis, must be known, as well as the potential of atypical presentations in case of *Pneumocystis jirovecii* (PCP) pneumonia when occurring in non-HIV immunocompromised patients. In all cases, underlying disorders must be considered as well as all the differential diagnoses. Overall, CT definitely helps clinicians to diagnose pulmonary infections and to make treatment decisions, especially in vulnerable patients.

Imaging plays a crucial role in the diagnosis of respiratory infections that are a source of high morbidity and mortality especially regarding the increasing number of elderly and immunocompromised patients (Franquet 2006; Herold and Sailer 2004). Despite its much greater sensitivity and specificity than plain film radiography (Heussel et al. 1999), computed tomography (CT) has not been recommended for the initial assessment in

C. Beigelman-Aubry (✉) • S. Schmidt
Diagnostic and Interventional Radiology,
University Hospital Lausanne, Lausanne, Switzerland
e-mail: Catherine.Beigelman-Aubry@chuv.ch;
Sabine.Schmidt@chuv.ch

U.J. Schoepf, F.G. Meinel (eds.), *Multidetector-Row CT of the Thorax*, Medical Radiology,
DOI 10.1007/978-3-319-30355-0_8

most cases. It must be performed when there is a high clinical suspicion of infection with normal, ambiguous, or nonspecific chest X-ray findings, especially in immunocompromised patients (Beigelman-Aubry et al. 2012), in case of atypical clinical and/or radiological presentations, or when an empyema or abscess is suspected (Stigl and Marrie 2013). CT is able to detect even subtle lesions, while demonstrating them earlier than chest X-ray, as well as associated abnormalities or underlying conditions. In addition, it may suggest alternative diagnoses, and can guide interventions to take specimens for microbiology, regardless of the applied technique, either bronchoalveolar lavage (BAL) or percutaneous, transbronchial, or transthoracic needle biopsy. CT is also the imaging modality of choice to monitor response to specific treatment. Although the major CT patterns of pneumonia may be individualized, there is no specific one caused by one particular microorganism. Moreover, multiple CT patterns frequently coexist in the same patient with pulmonary infection. In addition, the radiological appearance of the organism-specific infection can change depending on the degree of the patients' immunosuppression. The infective agents also vary with the type of immune deficiency. As the suggested diagnoses will very much depend on the individual setting, the conclusions drawn from the CT exam must always be integrated into the epidemiological, clinical data and laboratory tests and should result from a multidisciplinary approach. A first reminder of the most common types of pneumonias will be proposed before describing the technical approach and the main CT patterns encountered in routine practice.

1 Pneumonia Types

Community-acquired pneumonia (CAP), hospital-acquired pneumonia (HAP), ventilator-associated pneumonia (VAP), and healthcare-associated pneumonia (HCAP) are the main categories of pneumonias recognized by the currently accepted clinical classification of pneumonia (American Thoracic Society/Infectious Diseases Society of America 2005).

1.1 Community-Acquired Pneumonia (CAP)

Community-acquired pneumonia (CAP) is defined as an acute infection of the lung parenchyma acquired in the community, i.e., in outpatients or residents in long-term care facilities, >2 weeks before the onset of symptoms (Stigl and Marrie 2013). It can vary from a mild outpatient illness (Herold and Sailer 2004) to a more severe disease requiring hospital admission and, at times, intensive care (Niedemann 2015). The development of CAP may be related to either a defect in host defense, an exposure to an especially virulent pathogen, an overwhelming inoculum of microorganisms, or a combination of those factors (Stigl and Marrie 2013). Respiratory disorders, such as chronic obstructive pulmonary disease (COPD), cardiovascular disease, diabetes mellitus, chronic liver disease, HIV infection, and other forms of immune suppression, chronic kidney disease, old age, malignancy, any neurologic illness that predisposes to aspiration including seizures, alcoholic abuse, smoking, and splenectomy, are predisposing host conditions (Niedemann 2015). The diagnosis of CAP, usually based on the presence of cough, fever, sputum production, and/or pleuritic chest pain, is supported by infiltrates detected on the chest radiography in most cases. CT is therefore rarely required. Typical causative organisms of bacterial CAP include gram-positive bacteria such as *Streptococcus pneumoniae* (pneumococcus) that is responsible for approximately one-third of all cases of CAP, *Haemophilus influenzae*, and atypical pathogens, such as *Mycoplasma pneumoniae*, *Chlamydophila pneumoniae* (formally *Chlamydia*), and *Legionella* (Niedemann 2015). Viral agents, such as *influenza A* virus and *respiratory syncytial virus*, may also be involved, as well as fungi and parasites.

About 10–20 % of all adult patients hospitalized with CAP require admission to an intensive care unit. Severe CAP, usually defined by respiratory and/or circulatory failure, requires mechanical ventilation in 40–80 % of cases, with

concomitant septic shock in up to 50 % of cases and a high mortality rate (Stigl and Marrie 2013). Usual complications observed in severe CAP include empyema, lung abscess, pneumothorax, acute respiratory distress syndrome (ARDS), chronic respiratory failure requiring tracheostomy, major cardiac events such as acute coronary syndrome, and multisystem organ failure (Stigl and Marrie 2013).

1.2 Hospital-Acquired or Nosocomial Pneumonia (HAP), Ventilator-Associated Pneumonia (VAP), and Healthcare-Associated Pneumonia (HCAP) (American Thoracic Society/ Infectious Diseases Society of America 2005)

HAP or nosocomial pneumonia occurs 48 h or more after admission and does not appear to be incubating at the time of admission. Nosocomial pneumonia is the leading cause of death from hospital-acquired infections and most commonly affects intensive care unit (ICU) patients, particularly individuals requiring mechanical ventilation (Franquet 2008). VAP is a type of HAP that develops more than 48–72 h after endotracheal intubation. HCAP is defined as pneumonia that occurs in settings of a nonhospitalized patient with extensive healthcare contact, such as wound care, residency in a nursing home, or hemodialysis. The latter pneumonia is increasingly caused by multidrug-resistant (MDR) pathogens. Common pathogens of HAP, VAP, and HCAP are found in both the Proteobacteria and the Firmicutes phylum and include aerobic gram-negative bacilli (e.g., *Escherichia coli*, *Klebsiella pneumoniae*, *Enterobacter* spp., *Pseudomonas aeruginosa*, *Acinetobacter* spp.) and gram-positive cocci (e.g., *Staphylococcus aureus*, including methicillin-resistant *S. aureus* [MRSA], *Streptococcus* spp.) (Jones 2010). Nosocomial pneumonia due to viruses or fungi is significantly less common, except in the immunocompromised patient.

2 Technical Aspects of CT Procedures

Today, CT has to be performed on a multidetector row CT scanner acquiring around 1 mm-thick sections and using an exposure dose which needs to be carefully chosen. Low-dose (LD) CT may be used without impairing the diagnostic information of specific CT patterns, in particular in case of pulmonary fungal infections (Christe et al. 2012), and even ultralow dose (ULD) CT may be possible, according to the clinical context. Overall, the dose may be decreased depending on the size of anomalies to be detected. If they are greater than 1 cm, which is often the case for patients with cystic fibrosis and suspected of acute pulmonary infections, ULD-CT at a dose that nearly reaches that of a chest X-ray may demonstrate the abnormalities, provided that the series are reconstructed with the correct technical parameters (Fig. 1). These doses also apply to the follow-up of this young population that is exposed to frequent ionizing radiation procedures during the whole life. In other cases, LD-CTs with a CTDI of 2–3 mGy.cm in non-obese patients (Bankier and Tack 2010) are perfectly suited for the follow-up of infectious lung diseases (Fig. 2). A comparison with previous baseline examinations is always required to accurately assess the disease's evolution. Of importance, although ULD-CT with a mean radiation expose dose of 0.60 ± 0.15 mSv has been proven to provide acceptable image quality in case of pulmonary infections in febrile neutropenic patients with hematologic malignancy (Kim et al. 2014), caution must be taken due to potential pitfalls with LD-CT (Fig. 3). Multiplanar reformats with average intensity projection (AIP) post-processing of variable thickness may give rise to tomographic or chest X-ray appearance (Figs. 4 and 5) that may be compared with previous or following conventional chest X-rays. The use of maximum intensity projection (MIP) may optimize the detection of micronodules, which sometimes cannot be assessed by using thin slices alone (Fig. 6). It is also helpful to characterize micronodules as centrilobular ones with tree in bud appearance (Fig. 7), corresponding to a

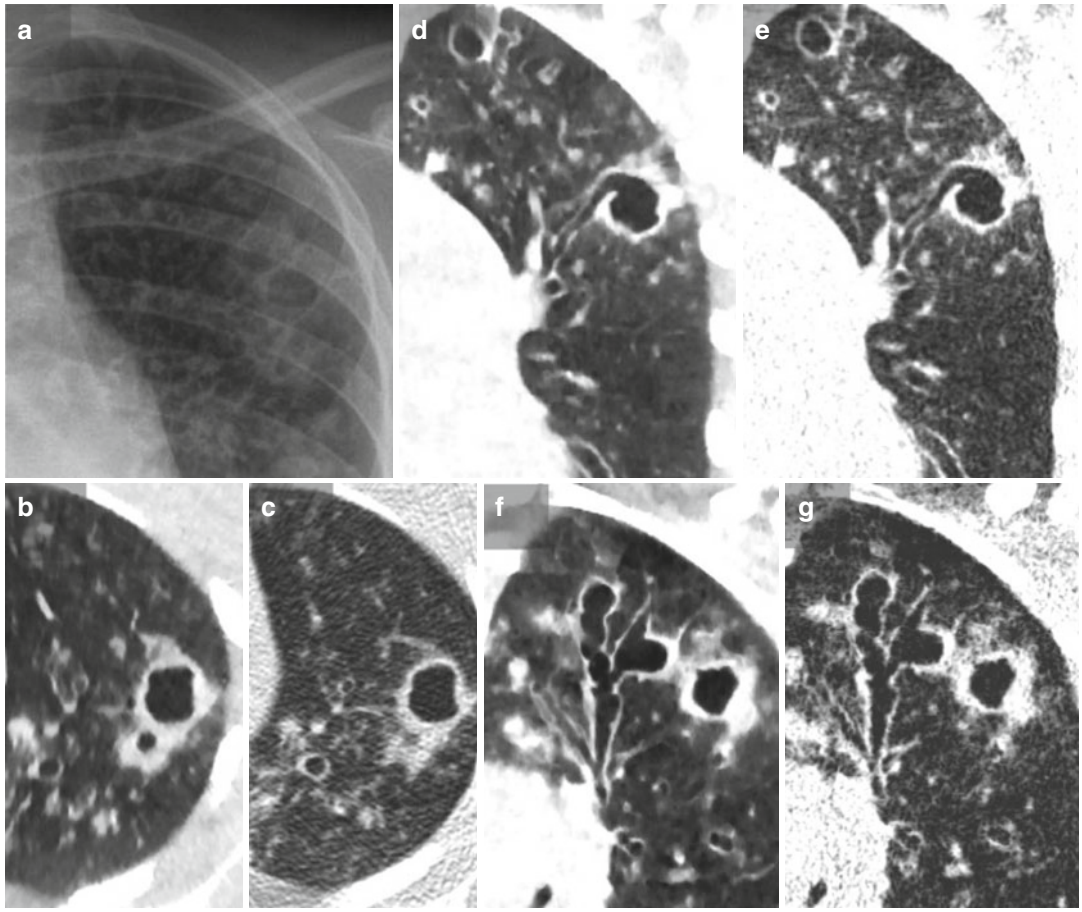

Fig. 1 Ultralow dose CT was performed because of the appearance of a cavity with an air-fluid level in the left axillary area on chest X-ray (**a**) in a 20-year-old female patient with cystic fibrosis and persistent symptoms due to *Staphylococcus aureus* and *Cepacia* infection despite antibiotic treatment. Axial sections reconstructed by using iterative reconstruction (IR) algorithm (**b**) and FBP with soft kernel and a slice thickness of 4 mm (**c**). Coronal reformatted image reconstructed by using IR (**d**, **f**) and filtered back projection (FBP) with soft kernel (e.g). The drainage bronchus of the abscess cavity (**d**, **e**) is clearly differentiated from the varicose bronchiectasis that are well assessed with a 3 mm-thick minimum intensity projection (mIP) reformat (**f**, **g**). Despite a slight distortion of the details seen on the axial image when using IR (**b**) compared with FBP (**c**), a substantial reduction of the noise is observed with IR (**d**, **f**)

bronchocentric distribution, or as ones with a random distribution as seen in miliary disease (Fig. 8) (Beigelman-Aubry et al. 2005). The use of minimum intensity projection (mIP) allows to accurately locate an abnormal area in order to guide a bronchoalveolar lavage (BAL) (Fig. 9), to differentiate bronchiectasis from a cavitary lesion (Fig. 1), to visualize the drainage bronchus in the latter situation, as well as to help to recognize a bronchopleural fistula.

CT may be performed without or with intravenous (IV) contrast, the latter especially to evaluate the necrotic component of a pneumoniae or abscesses (Fig. 9) and to optimize the differentiation from an empyema (Figs. 10 and 11). It has also been described as helpful for differentiation between a pulmonary angioinvasive mycosis and a bacterial pneumonia in high-risk hematologic patients by using volume perfusion CT (Schulze et al. 2012). IV contrast-enhanced CT is also

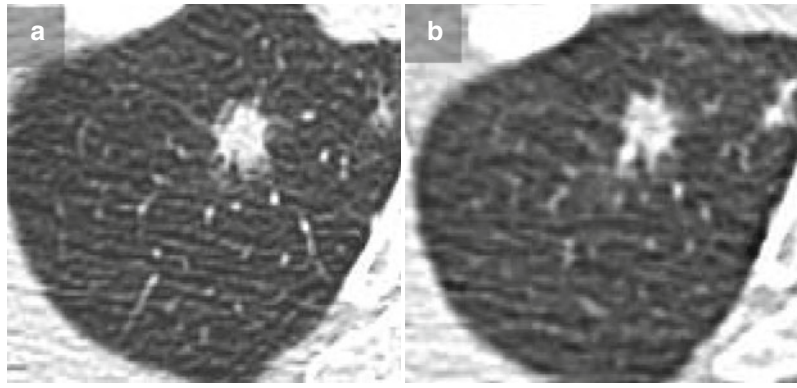

Fig. 2 Low-dose CT was performed for the follow-up of an angioinvasive aspergillosis in a 38-year-old woman with acute myeloid leukemia. The baseline CT (**a**) was performed with a CTDI of 5 and a DLP at 147 mGy.cm and the follow-up CT (**b**) with a CTDI of 2 and a DLP of 72 mGy.cm by using filter back projection reconstruction (FBP) with a soft kernel, without iterative reconstruction (IR) algorithm. Although a relative lesser image quality than the reference image, the disease's evolution may be perfectly assessed at less than half of the initial dose

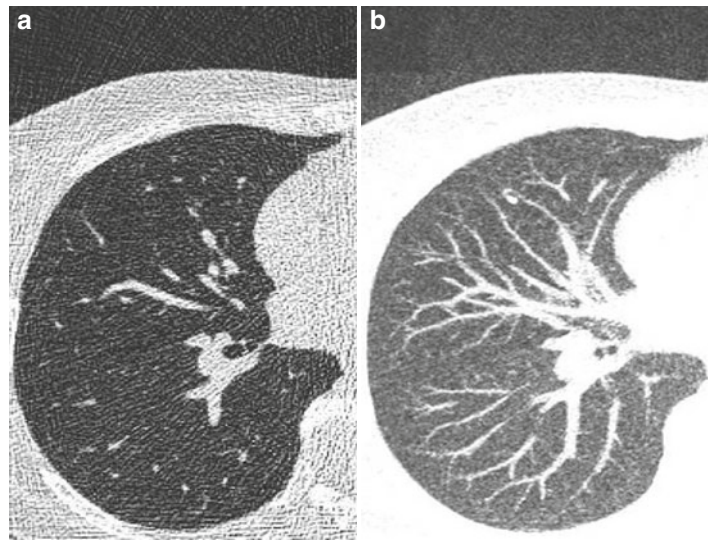

Fig. 3 Ultralow dose CT performed at 100 kV and 10 mAs corresponding to a CTDIvol of 0.4 mGy reconstructed with FBP and a lung kernel. Native thin axial section (**a**) and 10 mm-thick maximum intensity projection reformat (**b**) exhibit noise well seen outside of the chest wall. Such noise projected on the lung mimics micronodulation with random distribution that may simulate a miliary disease in a context of a febrile immunocompromised patient. Although IR is the method of reconstruction of choice with low-dose CT and available in most institutions today, such potential pitfalls with FBP and lung kernel must be known when IR is not available. This precludes the use of such doses in this setting

required in case of hemoptysis, being able to demonstrate enlarged bronchial and non-bronchial systemic arteries due to former tuberculosis or, less frequently, Rasmussen aneurysms (Fig. 12) occurring in the same situation as well as vessel involvement in case of fungal disease (Fig. 13). It may also highlight a concomitant thromboembolic disease.

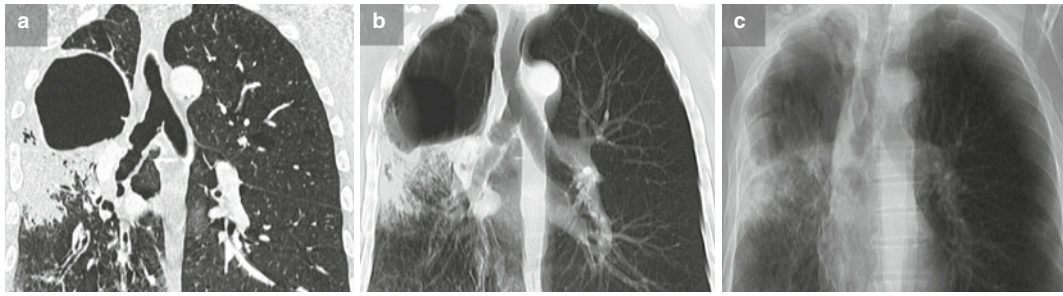

Fig. 4 Coronal reformatted images with progressive thickening of the slabs from 1 (**a**) to 30 (**b**) to 150 mm (**c**) thick slabs by using the average intensity projection (AIP) post-processing tool in a patient known for a voluminous bullae of the right apex of the lung with superimposed infectious alveolar consolidation. Note that the bullae is not easily seen on the chest X-ray rendering in (**c**), as it was the case with the conventional chest X-ray (not shown). The same limitation also occurs in case of cavitation that may be missed on conventional chest X-ray

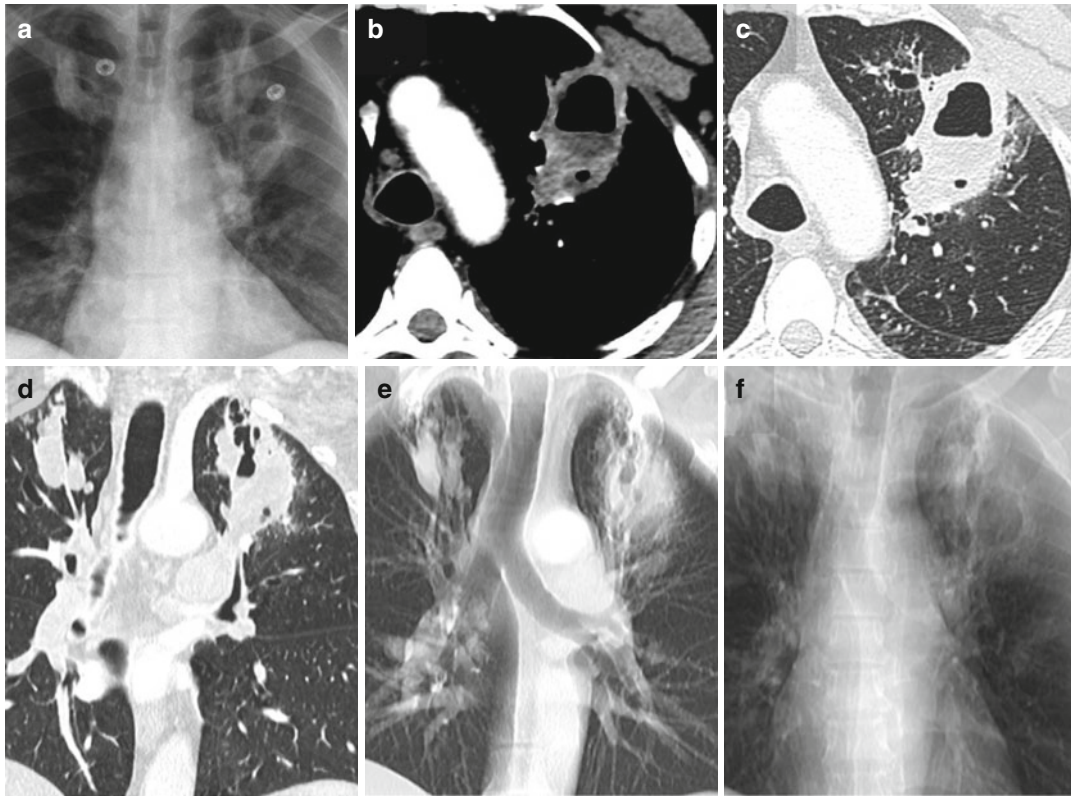

Fig. 5 A 60-year-old man suffering from bronchiectasis of unknown cause presented with fever and new respiratory symptoms related to an abscess due to a usually nosocomial germ, *Serratia marcescens* and *Cronobacter*, a gram-negative bacteria of the *Enterobacteriaceae* family. Chest X-ray (**a**) and axial CT section with IV contrast in mediastinal (**b**) and lung (**c**) windows show the abscess of the LUL with thick walls, a necrotic component and an air-fluid level. The coronal 1.5 mm (**d**), 30 mm (**e**), and 150 mm (**f**) thick AIP reformatted images allow for a better understanding of the opacities related to a bronchocele at the level of the RUL and the abscess situated close to a bronchiectatic area of the LUL

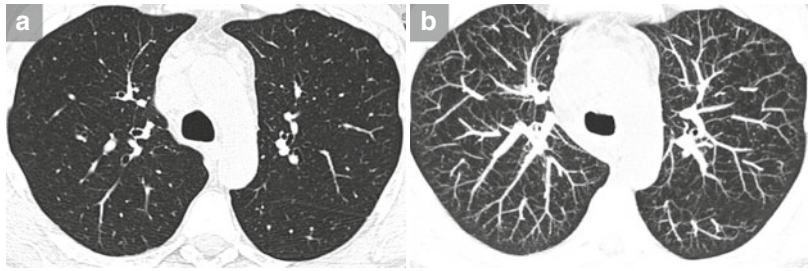

Fig. 6 16 mm-thick axial MIP image in a 58-year-old patient with Crohn disease under infliximab treatment. Although invisible on 1.25 mm-thick axial image (**a**), the MIP reformatted image (**b**) permits to detect micronodules with random distribution that were related to a miliary tuberculosis

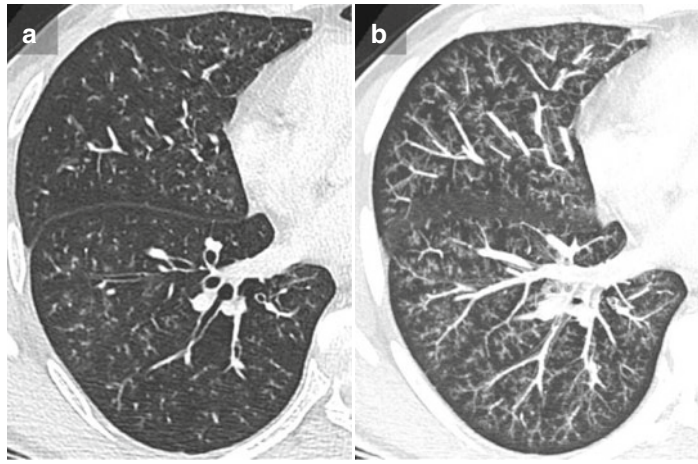

Fig. 7 Chest CT of a 36-year-old patient with ankylosing spondylarthritis treated by using anti-TNF alpha. Although numerous micronodules are visible on the thin axial section (**a**), their profusion and centrilobular distribution with tree in bud appearance related to *Mycoplasma pneumoniae* is more obvious when using 10 mm-thick MIP reformat (**b**). Note the sparing of the subpleural area typical of centrilobular distribution

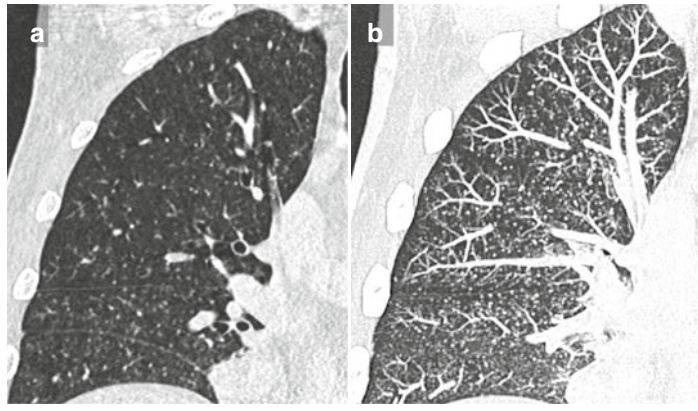

Fig. 8 Chest CT of a patient suffering from a Good's syndrome (thymoma with immunodeficiency) and miliary tuberculosis (TB). The thin coronal reformatted image (**a**) shows an apparent limited number of nodules, unlike the 10 mm-thick MIP reformat (**b**) that shows obvious micronodules with random distribution that were related to a hematogenous spread of TB

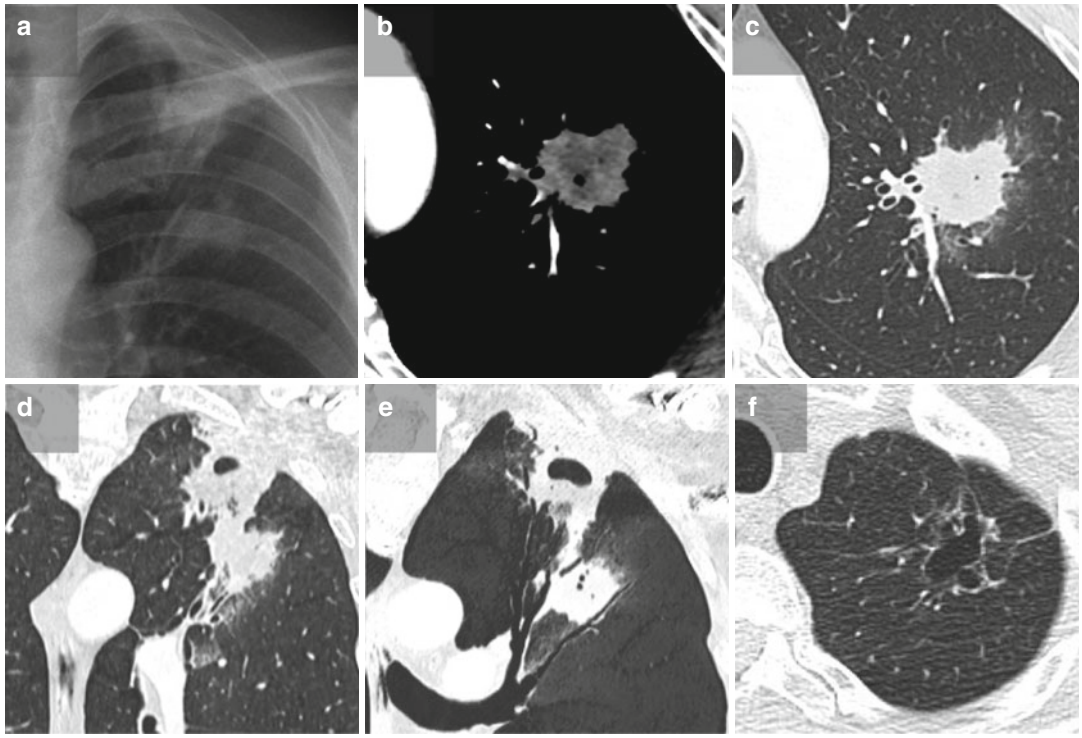

Fig. 9 Pulmonary abscess related to multisensible *Escherichia coli* in a 52-year-old male alcoholic and heavy smoker suffering from fever with respiratory symptoms resisting to first line of antibiotics. After an initial chest X-ray (**a**), a chest CT with intravenous (IV) contrast media injection was performed due to worsening of the status. It allowed for the exclusion of pulmonary embolism and demonstrated the necrotic component of a pulmonary abscess of the LUL on axial sections with mediastinal (**b**) and lung (**c**) windows. A coronal reformatted image (**d**) showed cavitation within the upper part of the lesion that was better assessed when applying 7 mm-thick mIP post-processing (**e**). The latter also allowed for demonstration of the drainage bronchus that helped the clinician to guide the BAL. A follow-up CT in axial sections (**f**) demonstrated the resolution of this lesion with a sequelae appearing as a cavity with lobulated margins with thin wall

3 Main CT Patterns

Although an overlap may be observed among the different patterns, with several patterns potentially occurring in various infectious disorders, the type of pneumonia may be suggested according to the predominant CT feature.

3.1 Alveolar Consolidation

Alveolar consolidation, which refers to an exudate or another product of disease replacing alveolar air and rendering the lung solid, appears as a homogeneous increase in pulmonary parenchymal attenuation obscuring the margins of vessels and airway walls. It may be associated with an air bronchogram, a pattern of air-filled bronchi on a background of high-attenuation airless lung (Hansell et al. 2008) that argues against the presence of a central obstructing lesion (Walker et al. 2014). Alveolar consolidation can be differentiated from atelectasis by the absence of direct and indirect signs of volume loss, such as fissural displacement, mediastinal shift, and diaphragmatic elevation. Alveolar consolidation is a major feature of infectious pneumonia as well as the predominant CT pattern of lobar pneumonia, bronchopneumonia, or diffuse alveolar consolidation.

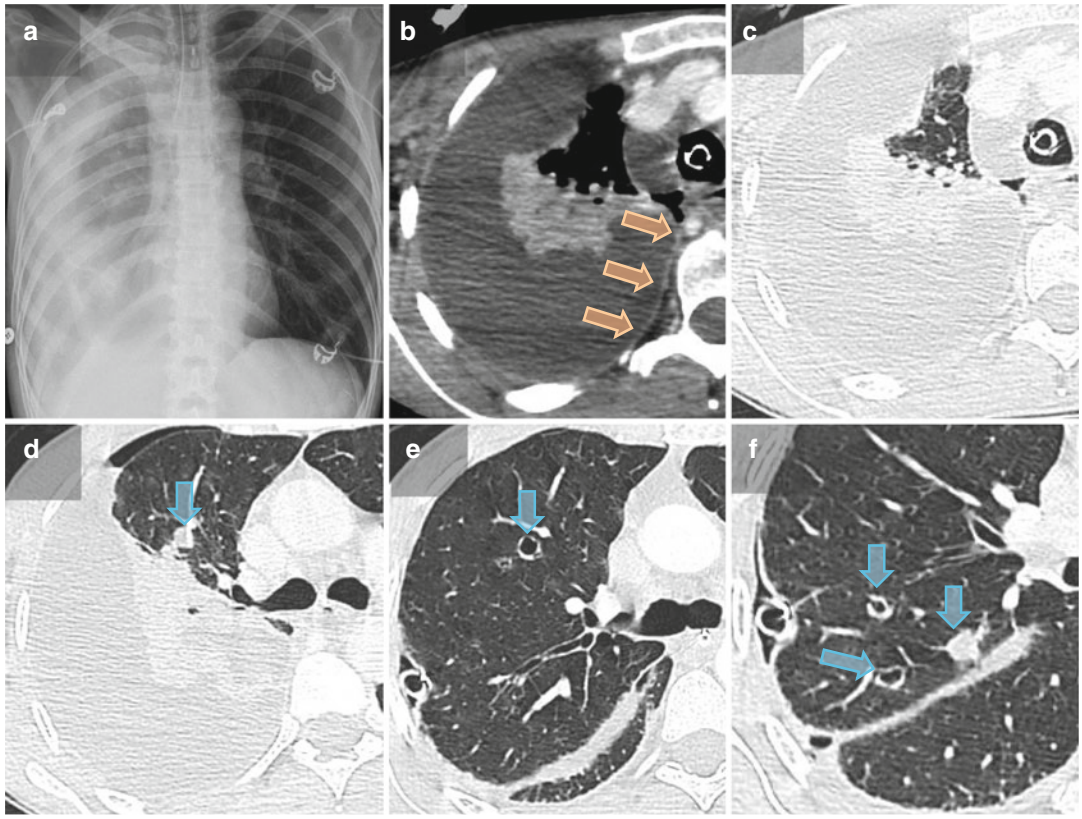

Fig. 10 Empyema with right pulmonary abscesses in a context of bronchoaspiration pneumonia due to *Streptococcus milleri* and *Fusobacterium necrophorum* in a 47-year-old patient known for previous drug abuse that was found unconscious at home. In addition to antibiotherapy, a thoracoscopy was performed with drainage of the empyema. The reference chest X-ray (**a**) shows a pleural effusion. The axial CT with IV contrast media administration in mediastinal (**b**) and lung (**c**) window at the level of the apical segment of the RUL performed at the same day confirms the pleural effusion with thin enhancement of the parietal pleura suggesting empyema with associated alveolar consolidation. An axial section in lung window at the level of the right upper lobe bronchus (**d**) of the reference CT and also a follow-up CT performed 3 days later (**e**) demonstrate the cavitation of a pulmonary abscess of the anterior segment of the RUL that appears solid in (**d**). An axial image at the level of the middle lobe (**f**) shows additional cavities and another solid nodule related to multiple abscesses

3.1.1 Lobar Pneumonia

Lobar pneumonia, characterized by an inflammatory exudate filling distal airspaces, typically begins in the lung area adjacent to the visceral pleura and spreads through the interalveolar pores of Kohn and the small airways from one segment to another (Muller 2003) respecting a centripetal pattern. Appearing as a single subpleural area of alveolar consolidation with blurred margins restricted to the area next to the fissures, it then progresses to a sublobar or lobar alveolar consolidation sharply demarcated by the interlobar fissure (Fig. 14) (Franquet 2008). An air bronchogram sign is strongly suggestive (Fig. 15) (Syrjälä et al. 1998). Ground-glass opacities adjacent to the alveolar consolidation corresponding to a partial filling of the alveoli may be observed (Fig. 16) (Tanaka et al. 1996). This aspect is the classical presentation of acute bacterial community-acquired pneumonia (CAP), mainly caused by *S. pneumoniae* (Bhalla and McLoud 1998), other agents responsible of complete lobar consolidation including *Klebsiella pneumoniae*, and other gram-negative bacilli, *L. pneumophila*, *H. influenzae*, and occasionally *M. pneumoniae* (Franquet 2008). A *P. jirovecii* infec-

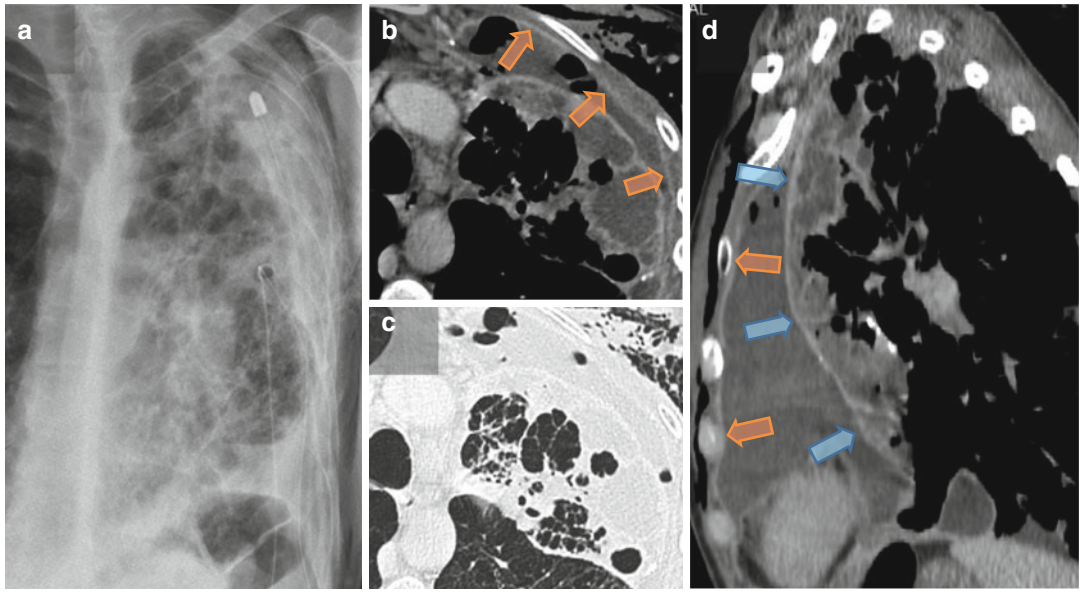

Fig. 11 A 46-year-old male drug abuser known for COPD presents with fever after bullectomy and pleurodesis performed for a spontaneous pneumothorax. Chest X-ray (**a**) and axial chest CT after IV contrast media injection in mediastinal (**b**) and lung (**c**) windows with sagittal reformat (**d**) allow for an easy differentiation between the parenchymal involvement with necrosis on an underlying bullous emphysema from empyema. The thickening of the pleura that is suggestive of empyema (*orange* and *blue arrows*) appears laterally as a continuous line internal to the ribs (*orange arrows*)

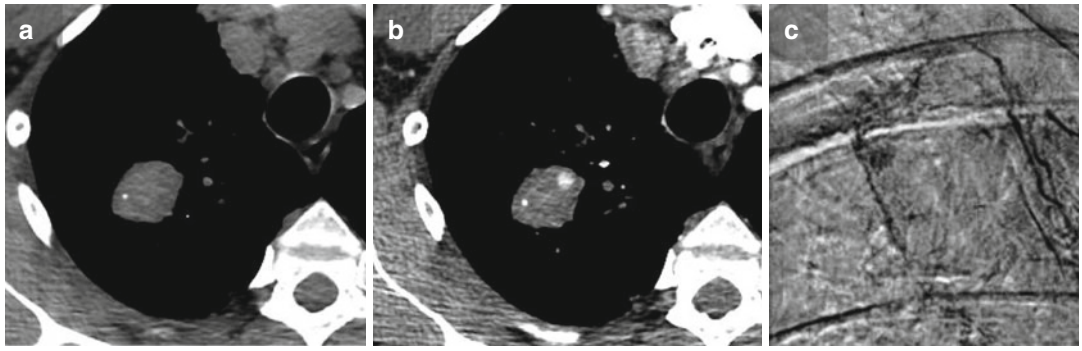

Fig. 12 Rasmussen aneurysm in a 35-year-old patient presenting hemoptysis 9 days after the initial diagnosis of TB. Axial CT without (**a**) and with IV contrast media injection (**b**) focused at the level of the RUL shows a vascular enhancement within the tuberculoma that was clearly differentiated from the calcification depicted without contrast. The selective angiogram of the right bronchial artery (**c**) shows the aneurysm that was immediately successfully embolized

tion, a fungal infection, or a mycobacteriosis has also to be considered in case of immunocompromised patients. An enlarged lobe with bulging fissures due to edematous engorgement may be observed, in particular with *K. pneumoniae* infection, with a current lower occurrence likely due to early treatment in case of suspected pneumonia (Walker et al. 2014).

The differential diagnosis includes aspiration pneumonia when the lower lung is affected, especially on the right side. Lobar or segmental consolidation may also be related to bronchial

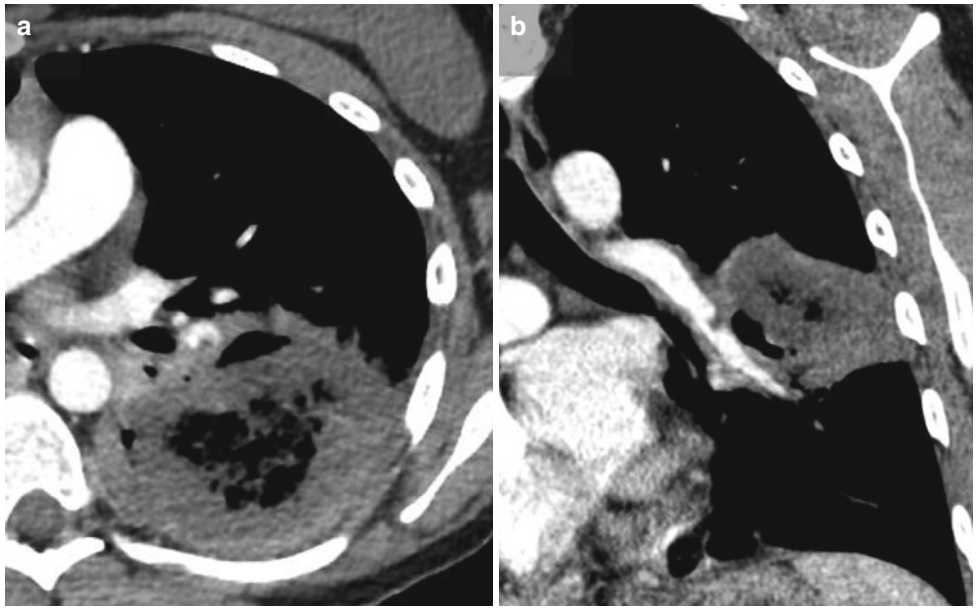

Fig. 13 Hemoptysis in the context of a mucormycosis in a 26-year-old woman suffering from acute lymphoblastic leukemia under antifungal prophylaxis. CT angiography in axial (**a**) and coronal oblique reformat (**b**) shows the vessel involvement originating from the necrotic parenchymal mass of the left lower lobe. This was confirmed after LLL lobectomy

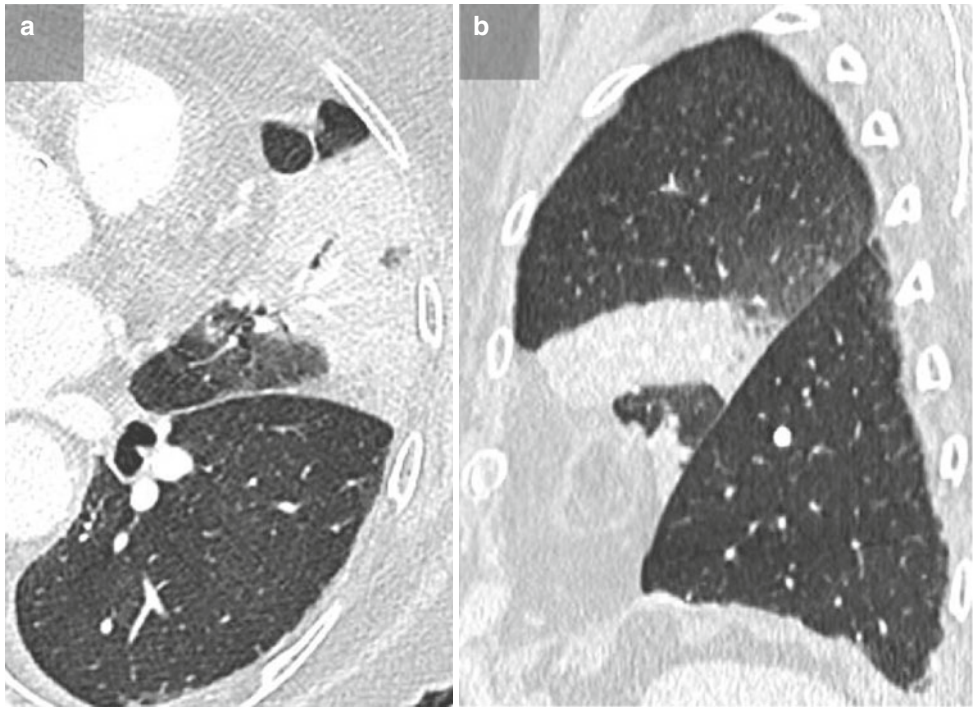

Fig. 14 Segmental pneumonia of the lingula in an 82-year-old woman. Axial CT scan focused at the level of the lower part of the LUL (**a**) and sagittal reformat (**b**) show an alveolar consolidation with a well-defined air bronchogram anterior to the great fissure

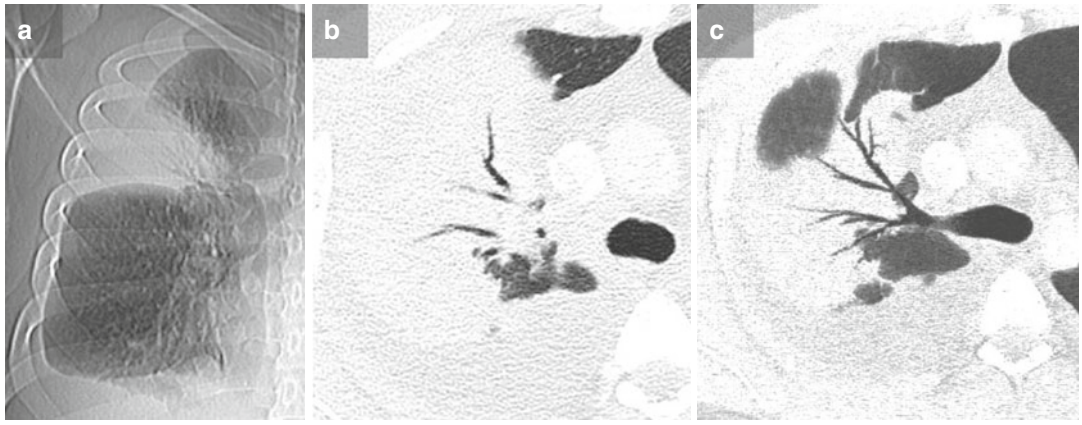

Fig. 15 Lobar pneumonia of the RUL related to *Streptococcus pneumococcus* in a 25-year-old smoker. Scout view (**a**) and axial CT image (**b**) show an alveolar consolidation with an air bronchogram. The 10 mm-thick mIP (**c**) permits to display the entire length of the bronchi from their origin within the alveolar consolidation. Although CT does not replace fiber-optic bronchoscopy, no obstructive lesion was detected by using CT

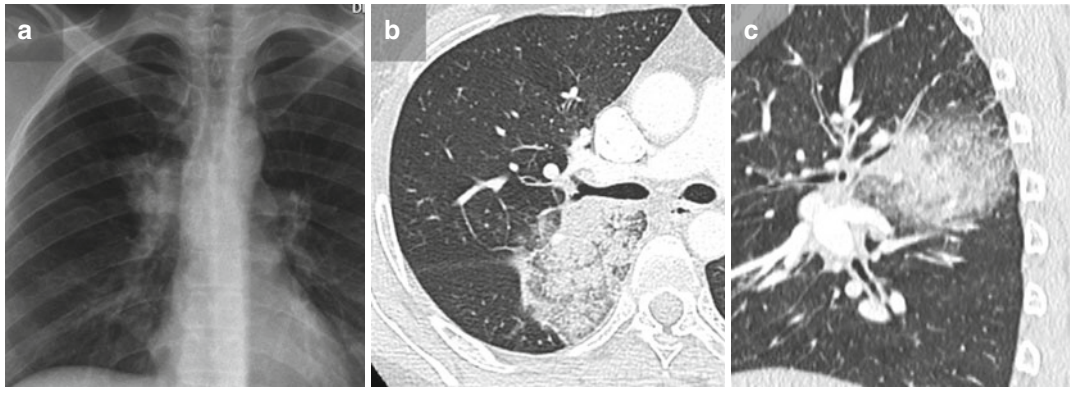

Fig. 16 Round pneumonia occurs in a 44-year-old man suddenly presenting with fever and chest pain and addressed to the emergency department. The chest X-ray (**a**) shows a right parahilar pseudo-tumoral opacity. Due to this atypical aspect, chest CT was performed on the same day. Axial CT image (**b**) and sagittal reformat (**c**) demonstrate a rounded alveolar consolidation of the posterior segment of the RUL and the apical segment of the RLL. Note the ground-glass opacity located around the alveolar consolidation reflecting the partial filling of the alveoli

obstruction, pulmonary hemorrhage, organizing pneumonia, acute fibrinous organizing pneumonia (Fig. 17), radiation pneumonitis, adenocarcinoma (Fig. 18), or lymphoma.

3.1.2 Bronchopneumonia or Lobular Pneumonia

Histologically, bronchopneumonia is characterized by a predominantly bronchiolar and peribronchiolar inflammation with a patchy distribution. Firstly, the adjacent alveoli are involved, followed by the lobules, segments, and/or lobes. An air bronchogram is usually absent. CT features include those of infectious bronchiolitis consisting of thickening of the bronchial walls, centrilobular nodules and tree-in-bud sign (Fig. 19) (see below), airspace nodules generally smaller than 1 cm in size related to the inflammatory spreading to the peribronchiolar alveoli with areas of ground-glass opacity or peribronchiolar consolidation (Fig. 20), and multifocal lobular, segmental, or lobar consolidation (Figs. 21 and 22). Bronchopneumonias are most commonly encountered in nosocomial infections and usually caused by gram-negative bacteria (GNB), especially

Fig. 17 Acute fibrinous organizing pneumonia (AFOP) in a 52-year-old patient suffering from plasmacytoid dendritic cells acute leukemia with febrile agranulocytosis. The noninfectious nature of the alveolar consolidation with peripheral ground-glass attenuation of the LUL was proven by a transbronchial biopsy performed under endobronchial ultrasonography (EBUS)

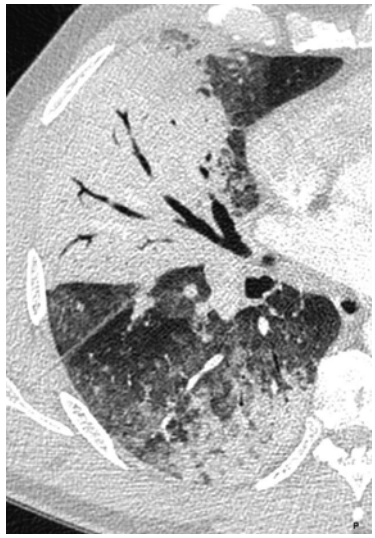

Fig. 18 Alveolar consolidation of the middle lobe related to an adenocarcinoma. The stretched appearance of the bronchi may suggest the diagnosis (Courtesy Pr Brillet, Bobigny, France)

P. aeruginosa or *E. coli*. Other commonly involved bacteria are *S. aureus* (Morikawa et al. 2012), *Haemophilus influenzae*, anaerobes, and some species of fungus, especially *Aspergillus* (Fig. 23). The latter as well as viruses (Franquet 2011) or atypical mycobacteriosis has to be considered when suggested by the individual clinical setting.

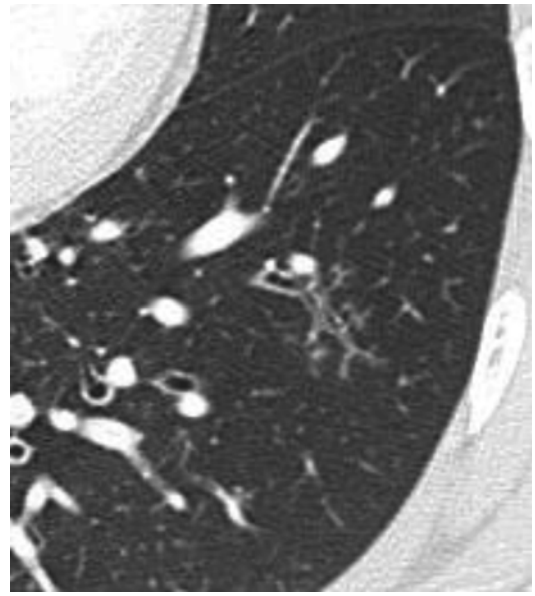

Fig. 19 Infectious bronchiolitis appears as thickening of the bronchial walls and centrilobular nodules with tree-in-bud sign

Bronchiectasis predominantly located at the level of the middle lobe and the lingula may be associated in case of *mycobacterium avium* complex (MAC) infection (Lady Windermere syndrome).

Differential diagnoses include organizing pneumonia, lymphoma, adenocarcinoma, radiation pneumonitis, acute hypereosinophilic syndrome, pulmonary alveolar proteinosis, granulomatous or inflammatory conditions, or lipoid pneumonia (Kjeldsberg et al. 2002).

3.1.3 Diffuse Alveolar Consolidation

Diffuse alveolar consolidation suggests diffuse alveolar damage (DAD), typically encountered in case of adult respiratory distress syndrome (ARDS). An air bronchogram sign is usually observed as well as small pleural effusions. *P. jirovecii* pneumonia (Festic et al. 2005) (Fig. 24) as well as uncommon, unusual, or exotic organisms can be involved. Nondependent anomalies are more related to pneumonia rather than lesions in the dependent lung (Beigelman-Aubry et al. 2012).

The differential diagnoses of infectious causes in case of diffuse involvement are pulmonary edema, noninfectious causes of DAD, and acute interstitial pneumonia.

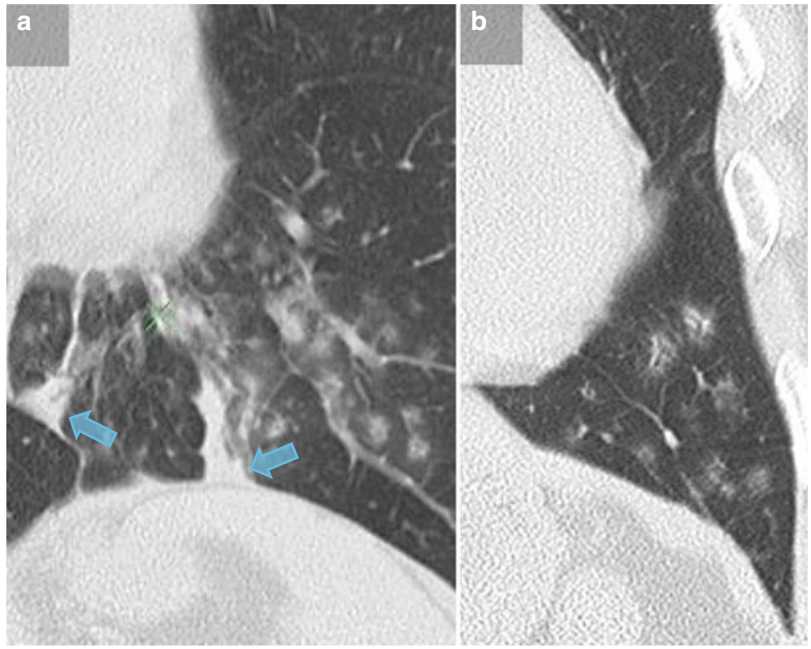

Fig. 20 Two consecutive coronal reformats in a 67-year-old man suffering from a bronchopneumonia show airspace nodules smaller than 1 cm with perinodular ground-glass opacity and patchy alveolar consolidation (*arrows*) (**a**) as well as peribronchiolar consolidation (**b**)

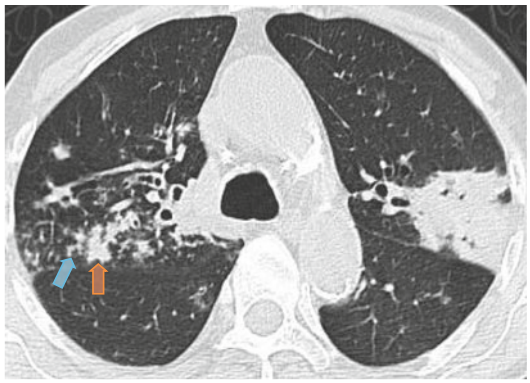

Fig. 21 Bronchopneumonia pattern appears on this axial section at the level of the upper lobes as bronchial wall thickening, centrilobular nodules with tree-in-bud sign (*blue arrow*), lobular (*orange arrow*), and segmental alveolar consolidation with multifocal and patchy involvement

3.2 Ground-Glass Opacity and Interstitial Pneumonia

Ground-glass opacity, a common but nonspecific finding, which refers to a hazy increased opacity of lung with preservation of bronchial and vascular margins (Hansell et al. 2008), is a major feature of interstitial pneumonia. Pathologically, it is characterized by a mononuclear inflammatory cellular infiltrate in the alveolar septa and the distal peribronchovascular interstitium (Muller 2003). This interstitial inflammatory reaction results from epithelial damage, with thickening of the peribronchial area and interlobular septa. Initially applied to different clinical and radiographic findings from those caused by *S. pneumoniae*, atypical pneumonia refers to an interstitial pattern that can be associated with dense consolidation.

The most common causes are viruses, *Mycoplasma pneumoniae*, *Chlamydia*, and *P. jirovecii*. In viral infections and in those caused by *M. pneumoniae*, ground-glass attenuation is associated with signs of cellular bronchiolitis and focal consolidation fitting with bronchopneumonia. When a predominant ground-glass opacity occurs in an immunocompetent patient, *respiratory syncytial virus* or varicella infection should be first considered. In immunocompromised patients, *P. jirovecii* (Thomas and Limper 2004)

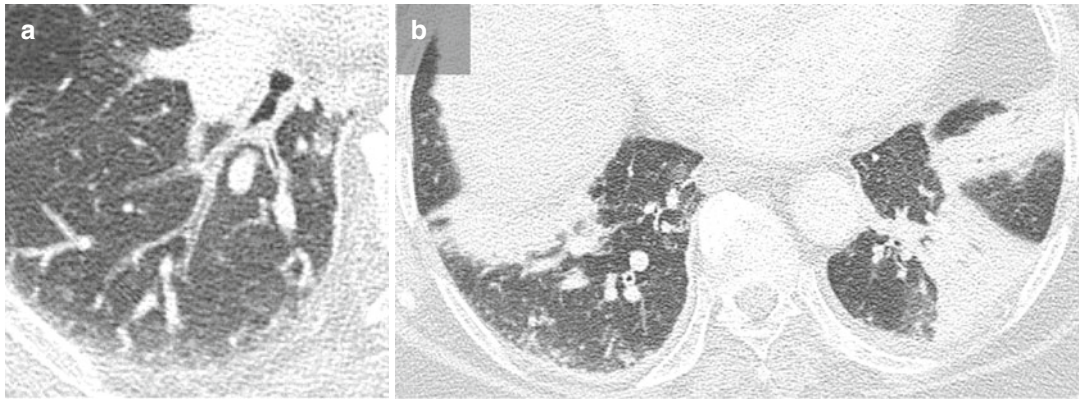

Fig. 22 CMV infection in a patient with renal graft appears as a bronchopneumonia pattern on two successive axial sections (**a**, **b**). The bronchial thickening in (**a**) is associated with bilateral segmental alveolar consolidations at the lung bases in (**b**)

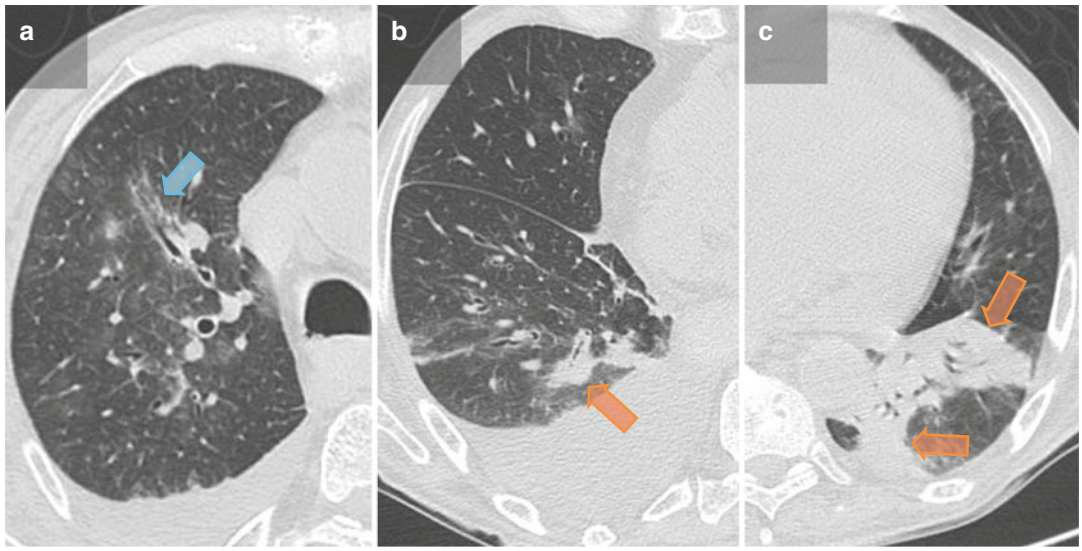

Fig. 23 Invasive airway aspergillosis. Three axial CT images show peribronchial ground-glass attenuation at the level of the RUL (*blue arrows*) with slight bronchial wall thickening and ill-defined nodules (**a**) and alveolar consolidation (*orange arrows*) in a peribronchial location at the level of the posterobasal bronchus of the RLL (**b**) and a segmental distribution in the LLL (**c**). This presentation of aspergillosis mainly concerns non-acute leukemia patients with a leukocyte count >100/mm^3

CMV (McGuinness et al. 1994) or *Mycoplasma* infection must be suggested. *P. jiroveci* infections typically present as ground-glass opacity sparing the pulmonary cortex that predominantly affects the upper region, especially in AIDS patients (Fig. 25). A crazy-paving sign, defined as a combination of ground-glass opacity and smooth interlobular septal thickening that resembles a masonry pattern used in walkways (Hansell et al. 2008), may be observed in infections, in particular with *Pneumocystis jirovecii* pneumonia and *influenza* (Walker et al. 2014). Pulmonary cysts or pneumatoceles within the same areas should suggest PCP (Fig. 26). In immunocompromised non-HIV-positive patients, features are less suggestive of the diagnosis, with rapid progression,

Fig. 24 Diffuse alveolar consolidation with air bronchogram and ground-glass opacity in a patient with autoimmune hepatitis treated with long-term steroids presenting with dyspnea and severe hypoxemia. This was related to a *Pneumocystis jirovecii* pneumonia. Note the pneumomediastinum in this mechanically ventilated patient staying in the intensive care unit who died from this severe infection with rapid deterioration

Fig. 25 *P. jirovecii* pneumonia in an AIDS patient appearing as ground-glass opacity sparing the pulmonary cortex and typically predominantly located at the upper region of the lungs

this being the result of severe or dysregulated inflammatory responses that are evoked by a relatively small number of *Pneumocystis* organisms (Chang et al. 2013; Tasaka and Tokuda 2012) (Fig. 27). In the latter category of patients, ground-glass opacities can also be caused by viral (Fig. 28) or pyogenic infection (Kang et al. 1996).

Peculiar aspects of GGO are seen with *the halo sign* (see below) and *the reversed halo sign*

Fig. 26 PCP pneumonia in an AIDS patient presenting with cough and fever. The crazy-paving appearance associated with cysts strongly suggests the diagnosis

Fig. 27 PCP pneumonia in an HIV-negative patient with a history of cerebral glioblastoma treated by surgery and radiochemotherapy. Axial CT shows ground-glass opacity predominating on the *left side* without sparing of the pulmonary cortex. The rounded hypoattenuated areas mostly correspond to centrilobular emphysema and not cysts that are rare in this condition

Fig. 28 Bilateral ground-glass opacity at the level of the upper lobes are related to a *Coronavirus* infection in a 72-year-old man known for a small cell carcinoma treated by radiochemotherapy

Fig. 29 Axial CT image shows a reverse halo sign in a 26-year-old woman known for an acute lymphoblastic leukemia that developed fever and cough with hemodynamic compromise despite antifungal prophylaxis. This was related to a mucormycosis (*Lichtheimia* spp) proven by transbronchial biopsy and panfungal PCR in the BAL

(RHS), defined as focal rounded area of ground-glass opacity surrounded by a crescent or complete ring of consolidation (Fig. 29) (Georgiadou et al. 2011). Histopathologically, the RHS has been associated to infarcted lung tissue, with a greater amount of hemorrhage at the periphery than at the center, with a frequent subsequent cavitation after neutropenia recovery (Wahba et al. 2008). Halo sign (HS) and RHS are highly suggestive of early infection by an angioinvasive fungus in severely immunocompromised patients. The former is most commonly associated with invasive pulmonary aspergillosis and the latter with pulmonary mucormycosis. An RHS may also be related to other infectious diseases, in particular invasive aspergillosis, tuberculosis, or paracoccidioidomycosis (Georgiadou et al. 2011).

The differential diagnosis of ground-glass attenuation is wide, especially in immunocompromised patients. It can be related to drug-induced toxicity (Fig. 30), alveolar hemorrhage, post-radic changes, pulmonary edema, organizing pneumonia, or hypersensitivity pneumonitis.

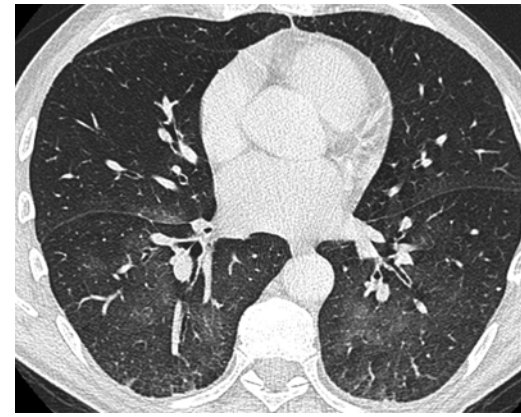

Fig. 30 Pulmonary hemorrhage in a 65-year-old woman known for an acute myeloid leukemia with thrombocytopenia appears as a perihilar ground-glass opacity predominantly located at the level of the lower lobes

An RHS may also be observed in numerous conditions including granulomatosis with polyangiitis, organizing pneumonia (Georgiadou et al. 2011), or pulmonary infarct (Fig. 31).

3.3 Nodular Pattern

3.3.1 Micronodules

Micronodules in an infectious setting, with a diameter lower than 6 mm, may appear with a centrilobular (bronchogenic) or miliary (hematogenous) distribution.

- Bronchogenic distribution presents as nonhomogeneous centrilobular micronodules that spare the subpleural space with a location at least 3 mm from the pleura and that are associated with a tree-in-bud pattern, defined as centrilobular branching structures that resemble a budding tree (Hansell et al. 2008). This presentation may be seen in bacterial, fungal, viral, mycobacterial, or mycoplasma (Fig. 7) infections. In postprimary (reactivation) tuberculosis, centrilobular micronodules and linear branching opacities have a dense attenuation and distinct margins. These features are readily associated with cavitation, predominantly localized in the apical and posterior segments of the superior lobes and the superior segment of the

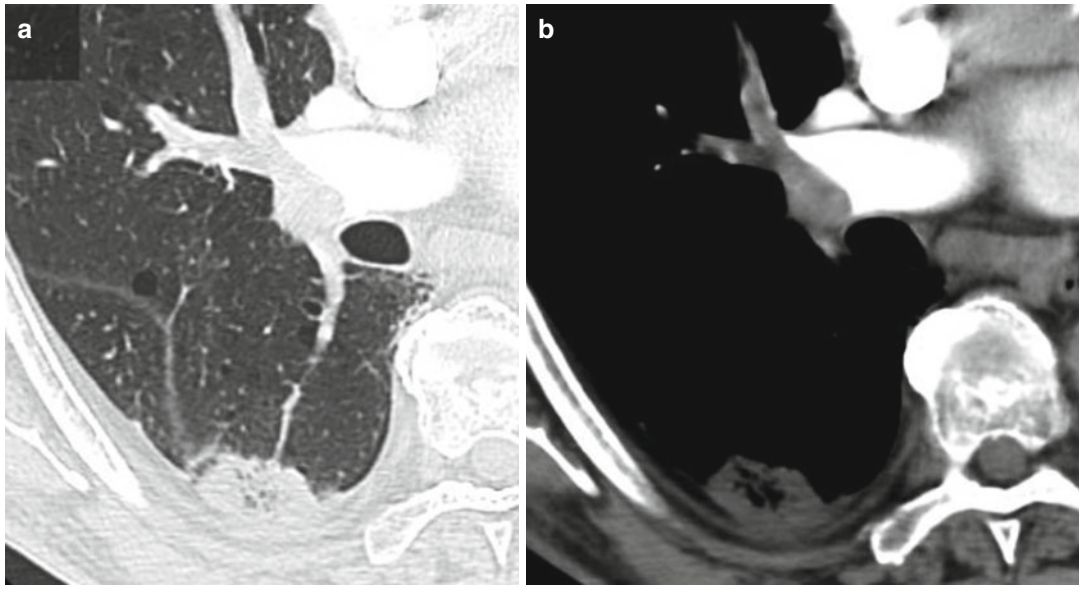

Fig. 31 Pulmonary infarct appears as a reverse halo sign in a 93-year-old patient with bilateral pulmonary emboli as nicely seen on axial CT section in lung (**a**) and mediastinal (**b**) windows

lower lobes in this setting (Fig. 32). *Aspergillus* bronchiolitis and/or bronchopneumonia must be considered in immunocompromised patients (Logan et al. 1994).

- A hematogenous miliary pattern in case of random distribution may suggest tuberculosis (Figs. 8 and 33), histoplasmosis, candidiasis, blastomycosis, or a viral cause (*CMV*, *herpes*, *varicella*) (Fig. 34), especially in immunocompromised patients.

The differential diagnosis of infectious micronodules is miliary metastatic disease in case of micronodules with a random distribution. Uncommonly, multiple centrilobular nodules may be related to vascular lesions as embolized tumor or foreign material (Walker et al. 2014). Other differential diagnoses of centrilobular nodules include hypersensitivity pneumonitis or vasculitis.

3.3.2 Nodules

Pulmonary nodules of infectious nature, sometimes cavitated, are most commonly seen in nosocomial pneumonia and in immunocompromised patients. They may be due to nocardiosis, tuberculosis, and angioinvasive aspergillosis (Althoff Souza et al. 2006) in neutropenic patients, *Cryptococcus neoformans*, *Coccidioides immitis*, *Blastomyces* sp., or atypical mycobacteriosis (Oh et al. 2000; Franquet et al. 2003). Less often, infections such as candidiasis (Fig. 35), legionella, or Q fever may be considered if suggested by the individual setting. They must be differentiated from noninfectious causes including malignancy (Fig. 36).

Nodules with a peripheral ground-glass halo refer to the *halo sign* (HS), which is a CT finding of ground-glass opacity surrounding a nodule or a mass (Hansell et al. 2008). Although inconstant, with a reported incidence of ranging from 25 to 95 % among neutropenic patients with hematological malignancies (Georgiadou et al. 2011), the HS strongly suggests an early invasive aspergillosis in patients with severe neutropenia (Fig. 37), in association with wedge-shaped areas of subpleural consolidation. Furthermore, initiation of antifungal treatment on the basis of the identification of an HS by chest CT appears associated with a significantly better response to treatment and improved survival (Greene et al. 2007). In invasive aspergillosis, these nodules typically become larger during neutrophil

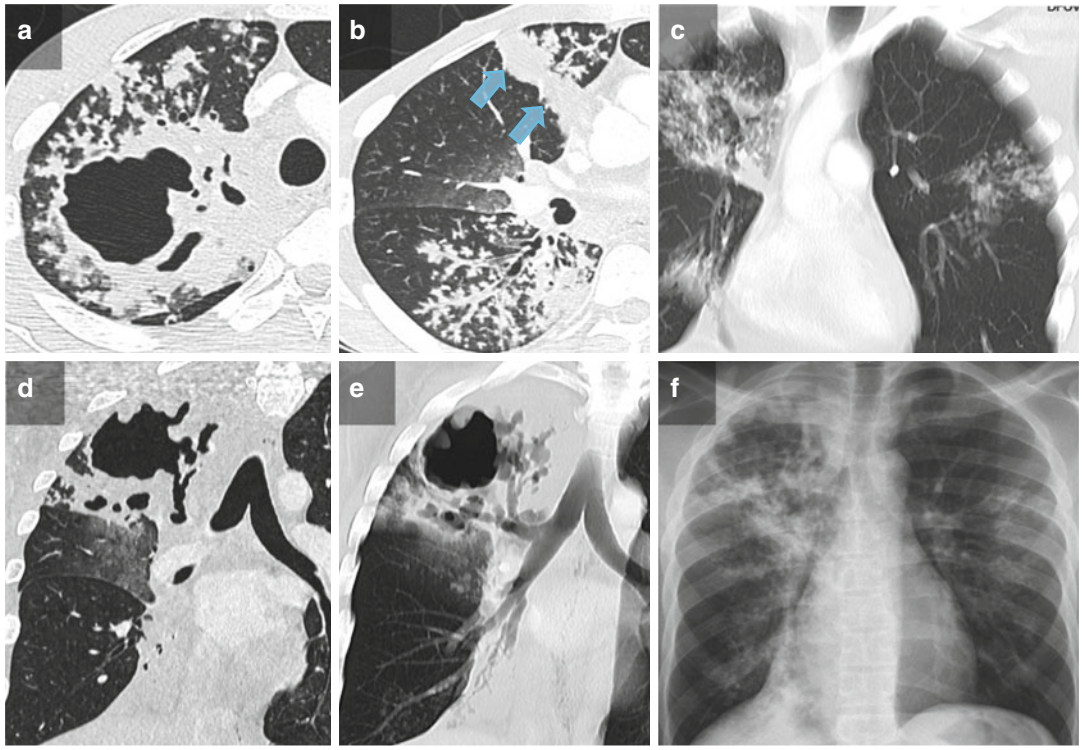

Fig. 32 Postprimary (reactivation) tuberculosis in a 37-year-old man, native of Cameroun, complaining about cough, weight loss, and night sweats for 3 months. Axial CT image at the level of the RUL (**a**) shows the typical hallmarks of reactivation TB including cavities, surrounded by thick and irregular borders, and dense centrilobular nodules with sharp margins predominantly located at the level of the apical and posterior segments of the upper lobes and the apical segment of the lower lobes. A 4 mm-thick MIP axial reformat at the level of the apical bronchus of the RLL (**b**) demonstrates typical centrilobular nodules with sparing of the subpleural space (3 mm) and lobular consolidation of the anterior segment of the RUL (*arrows*). Two consecutive coronal reformats 20 mm-thick AIP (**c**, **e**) and thin coronal slice at the level of the drainage bronchus of the largest cavity of the RUL (**d**) allow for a complete understanding of the appearance seen on chest X-ray (**f**)

engraftment (Barnes and Marr 2007) and/or during the first 10 days of therapy (Caillot et al. 2001). Histopathologically, the HS represents a focus of pulmonary infarction surrounded by alveolar hemorrhage, secondary to invasion by *Aspergillus* of small and medium-sized pulmonary vessels causing thrombosis and subsequent ischemic necrosis of the lung parenchyma (Georgiadou et al. 2011). The same appearances have been reported in numerous infectious pulmonary diseases such as observed with *Mucorales*, *Candida*, *herpes simplex virus*, *cytomegalovirus*, *varicella-zoster virus*, mycobacterial infections, bacterial pneumonia, or septic emboli (Fig. 38). The differential diagnoses of non-infectious nodules with an HS include granulomatosis with polyangiitis, cryptogenic organizing pneumonia, adenocarcinoma, angiosarcoma, Kaposi's sarcoma in association with spiculated nodules, and hemorrhagic metastases (Georgiadou et al. 2011).

Cavitated nodules can be related to septic embolism. The primary source of infection is tricuspid endocarditis, especially in intravenous illicit drug use, peripheral thrombophlebitis, venous catheter, and pacemaker wires. The mechanism includes endothelial damage combined with the formation of crumbling thrombi containing infective agents. Turbulences caused by the circulating blood detach fragments of thrombus which then migrate to the peripheral

Fig. 33 Miliary tuberculosis with multisystemic involvement in an HIV-positive CDC stage three patient highly immunosuppressed with CD4 level at 64 c/mm^3. Axial CT scan shows diffuse tiny micronodules with ground-glass opacity leading to alveolar consolidation at the level of the apical segment of the RLL. Such an involvement may result in a respiratory distress syndrome (ARDS)

pulmonary arteries with consecutive obstruction. Ischemia then results in infarction and/or hemorrhage and the organisms release toxins causing parenchymal necrosis (Muller 2003). Nodules related to septic emboli are mainly peripheral and basal with blurred margins. A simultaneous appearance of solid nodules and nodules with variable size cavitations (Fig. 38) as well as subpleural wedge-shaped consolidation may be seen (Franquet 2008). The nodules often appear to have a vessel leading into them on axial views – the so-called "feeding vessel" sign – corresponding to the pulmonary vein, whereas most arteries have a lateralized trajectory around the nodule (Dodd et al. 2006) (Fig. 39).

Other causes of cavitated nodules include granulomatosis with polyangiitis and cavitated metastases.

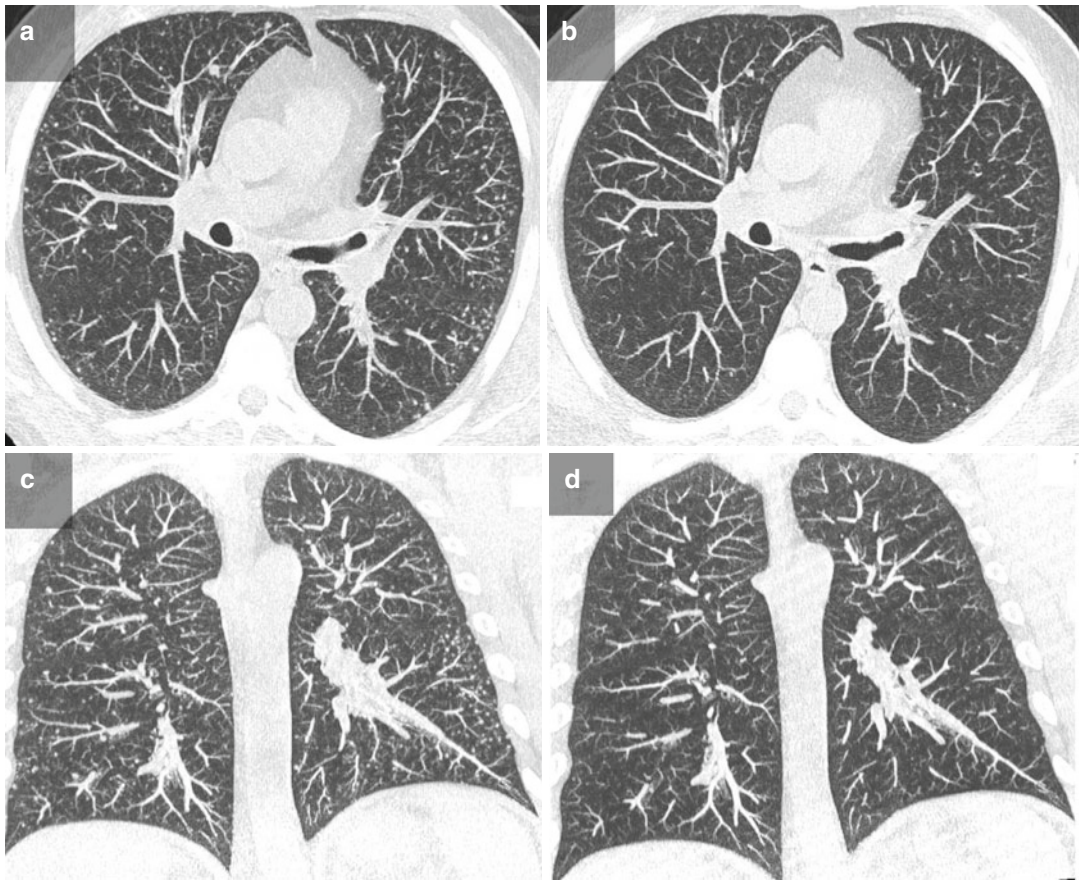

Fig. 34 A 50-year-old man developing a varicella without respiratory symptoms. Axial (**a**) and coronal (**b**) 10 mm-thick MIP images of a CT performed due to suspicion of pulmonary nodules on the chest X-ray show micronodules with random distribution that almost completely disappeared at the follow-up 3 months later (**c**, **d**)

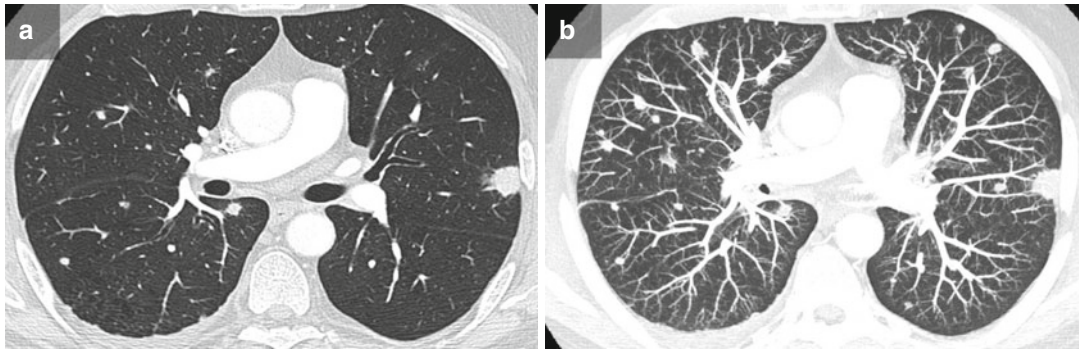

Fig. 35 Pulmonary and hepatosplenic candidiasis in a 62-year-old patient with an acute myeloid leukemia treated by chemotherapy. Axial CT image of 1 mm (**a**) and 15 mm-thick MIP (**b**) shows multiple nodules of various sizes with random distribution. The added value of MIP in the assessment of the detection and evaluation of profusion of nodules is undeniable

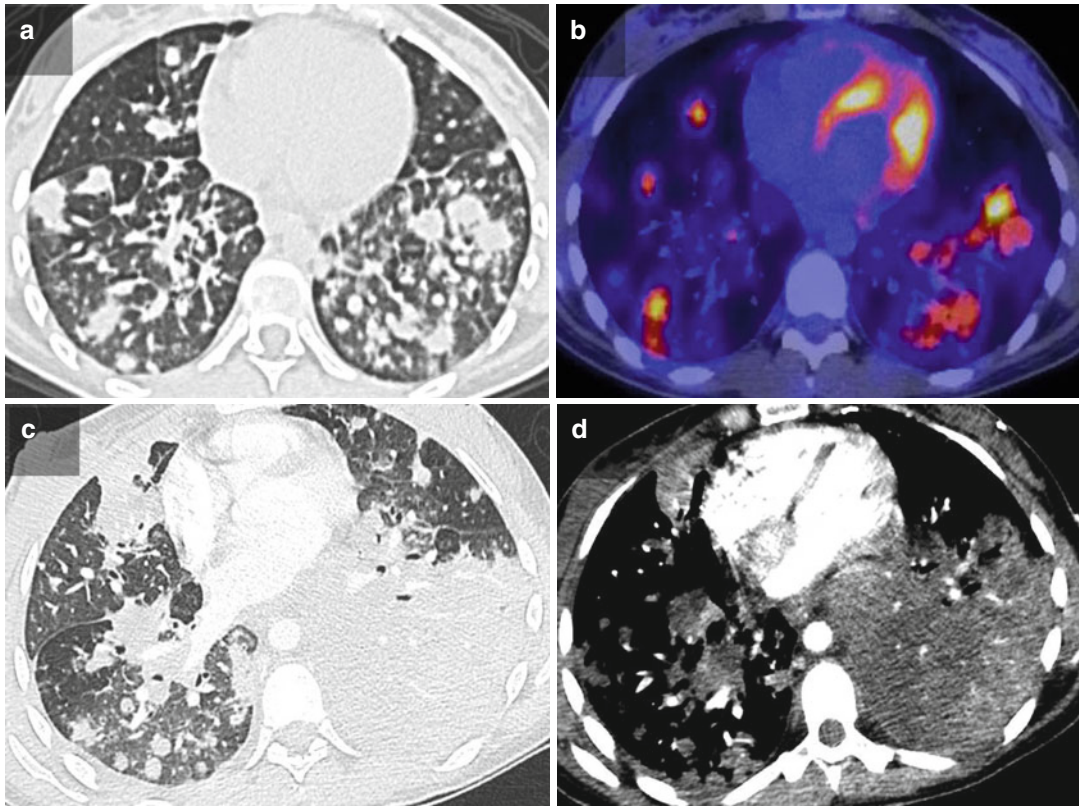

Fig. 36 A 24-year-old woman is known for a recurrence of Hodgkin's lymphoma appearing on the PET-CT (**a**, **b**) as multiple pulmonary nodules. A necrotic bronchopneumonia occurring 2 months later presents as bilateral alveolar consolidation superimposed on the preexisting nodules (**c**, **d**) that lead to a septic shock with death of the patient. This case reinforces the usefulness of evaluation of previous imaging features

3.4 Cavities

Cavities may be observed in case of necrotizing pneumonia or pulmonary gangrene, abscesses, or pneumatoceles.

Fig. 37 Angioinvasive aspergillosis in a 27-year-old woman appears as nodules with peripheral ground-glass opacity at the apex of the LUL

3.4.1 Necrotizing Pneumonia or Pulmonary Gangrene

Necrotizing pneumonia or pulmonary gangrene presenting with hypoenhancing geographic areas of low lung attenuation and cavitation is frequently seen before frank abscess formation (Walker et al. 2014). They can be encountered in various situations such as acute CAP, pulmonary tuberculosis (Fig. 32), atypical mycobacteria (Fig. 40), anaerobic bacteria, and angioinvasive or chronic fungal infections. Unilateral or bilateral areas of consolidation, multiple expanding usually thick-walled cavities containing or not aspergillomas and concomitant pleural thickening, suggest chronic cavitary pulmonary aspergillosis. In young patients with no medical history, an infection caused by *S. aureus*, Panton-Valentine leukodicin secretor, that can be severe and rapid in onset with a poor prognosis should routinely be investigated. Bilateral consolidations of the superior lobes followed by the development of coalescent lucencies are commonly seen. An air-crescent sign may also be present (see below).

Cavitation may occur in other conditions including malignancy and lung infarction (Walker et al. 2014).

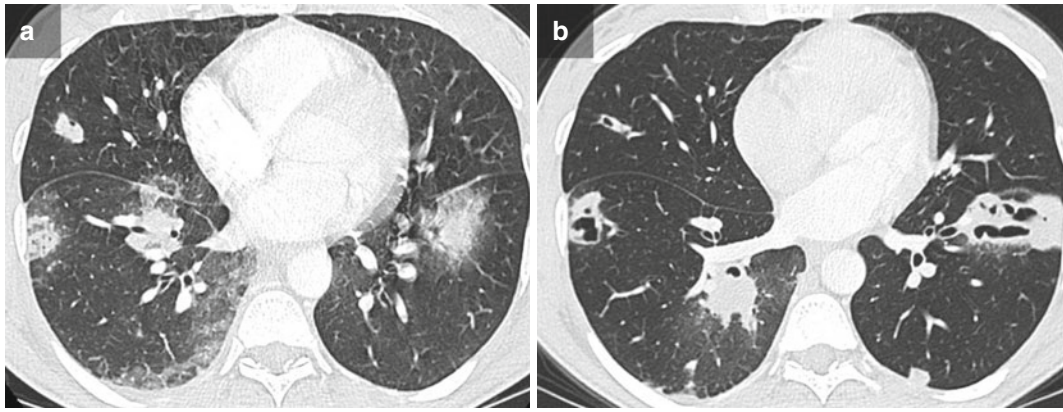

Fig. 38 Septic emboli in a 31-year-old female; HIV-negative drug abuser, known for chronic HCV and IV cocaine injections, presents with fever, shivering, and episodes of hemoptysis. Blood cultures were positive for *Staphylococcus aureus* with a 2 cm vegetation at the level of the tricuspid valve causing marked tricuspid insufficiency. Axial CT sections at baseline (**a**) and 8 days later (**b**), respectively, show multiple nodules with peripheral ground-glass opacity (**a**) that secondary cavitated. The latter is a usual finding with *Staphylococcus aureus* infection

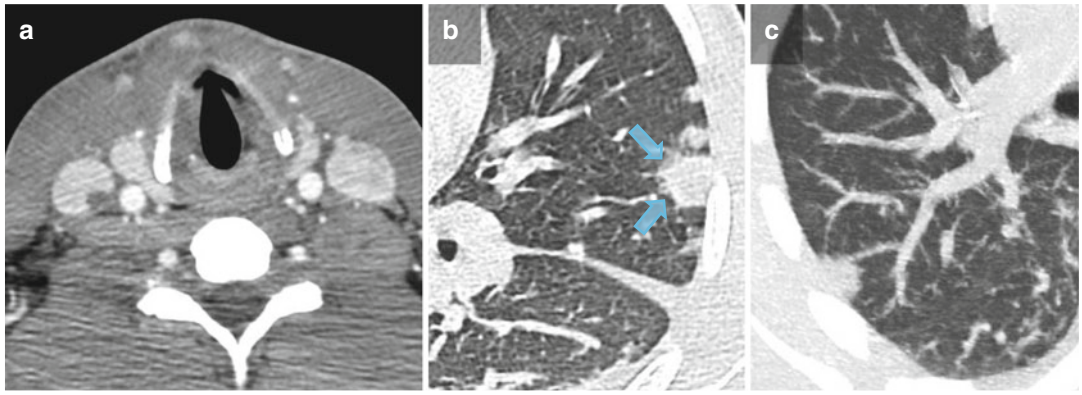

Fig. 39 Lemierre syndrome in a 21-year-old man suffering from a sore throat with jugular vein thrombosis well depicted by CT with contrast media injection (**a**) and septic embolism appearing as peripheral nodules of various sizes with wedge-shaped consolidation (*arrows*) and slight peripheral ground-glass opacity on axial CT image (**b**). The 8 mm-thick MIP image (**c**) shows the lateralized trajectory of the artery around the nodule

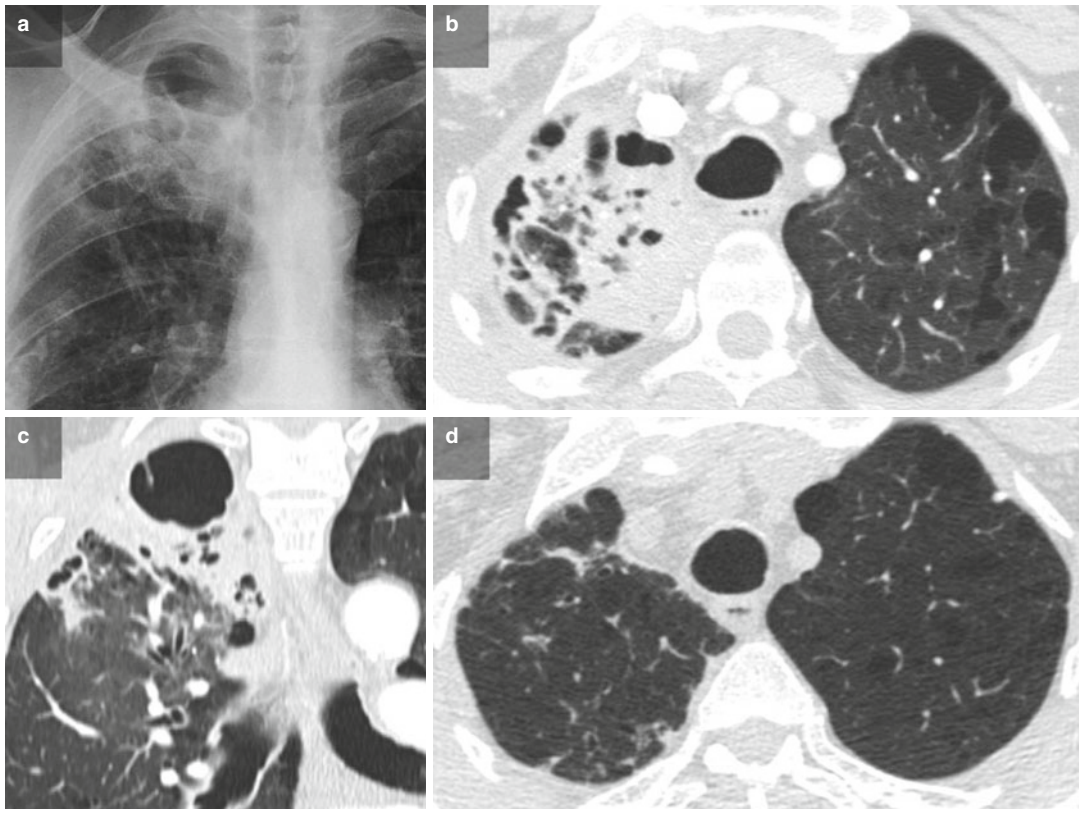

Fig. 40 *Mycobacterium xenopi* infection in a COPD patient. Chest X-ray (**a**), coronal reformat (**b**), and axial CT at the level of upper lobes (**c**) show an alveolar consolidation with cavities of various sizes that almost totally resolved on the follow-up CT performed 1 year later (**d**)

3.4.2 Pulmonary Abscess

A pulmonary abscess may be single or multiple, with a characteristic spherical shape. It measures between 2 and 6 cm in diameter, demonstrates a central hypoattenuation (Fig. 9) or cavitation representing localized necrotic cavity, contains pus, and demonstrates peripheral enhancement after intravenous contrast medium injection, without or with an air-fluid level (Fig. 5). It usually displays an acute angle when it intersects with an adjacent pleural surface. Consolidation in the adjacent parenchyma occurs in half of all cases (Muller 2003). Bronchopulmonary fistula may be observed. As the most frequent cause of lung abscess is aspiration, the most common localizations are the posterior segment of an upper lobe or the superior segment of a lower lobe (Muller 2003). Bilateral involvement that predominantly affects the lung bases with abscess formation suggests a *P. aeruginosa* infection. Infections caused by anaerobic bacteria are commonly encountered, abscesses caused by *S. aureus*, *K. pneumoniae*, and *P. aeruginosa* being associated with higher mortality (Francis et al. 2005).

3.4.3 Air-Crescent Sign

The air-crescent sign, defined as a collection of air in a crescentic shape that separates the wall of a cavity from an inner mass, firstly suggests an *Aspergillus* colonization of preexisting cavities, i.e., an aspergilloma (Fig. 41). An aspergilloma may also be manifested as an irregular spongeworks or fungal strands forming a coarse and irregular network within a cavity. An air-crescent sign also suggests the retraction of a central necrotic mass after recovery of the bone marrow in a rather late stage of angioinvasive aspergillosis (De Marie 2000) (Fig. 42). It may also occur in mucormycosis (Fig. 43), tuberculosis, granulomatosis with polyangiitis, intracavitary hemorrhage, and cavitary lung cancer (Fig. 44) (Hansell et al. 2008).

3.4.4 Septic Emboli

Septic embolism may appear as cavitated nodules (see cavitated nodules).

3.4.5 Pneumatoceles

Pneumatoceles manifest as single or multiple approximately round thin-walled and gas-filled spaces in the lung (Hansell et al. 2008) (Fig. 10). These lucencies are associated with a recent infection and usually transient, progressively increasing in size over the following days and weeks and then resolving after weeks or months. They are most likely due to bronchial drainage of necrotic parenchymal tissue, followed by a check-valve airway obstruction. They usually occur in *P. jirovecii* infections occurring in patients with acquired immune deficiency syndrome (AIDS) (Fig. 26) or in case of previous *S. aureus* pneumonia, but they can also be seen with other infections including *E. coli* and *S. pneumoniae* (Beigelman-Aubry et al. 2012).

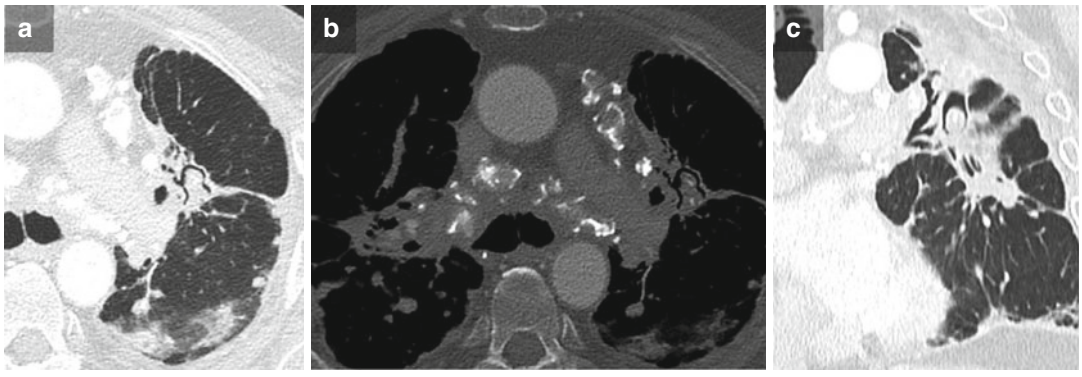

Fig. 41 Aspergilloma developing in a cavity in a 69-year-old man with a history of stage IV sarcoidosis who complained of hemoptysis. The treatment consisted of antifungal therapy and bronchial embolization followed by a left upper lobectomy. Axial CT section in lung window (**a**) at the level of the LUL shows the air-crescent sign. Axial CT section on bone window (**b**) at the same level demonstrates the calcified lymph nodes related to sarcoidosis and the slight calcifications within the aspergilloma. The coronal reformat (**c**) shows the typical dependent location of the aspergilloma within the cavity

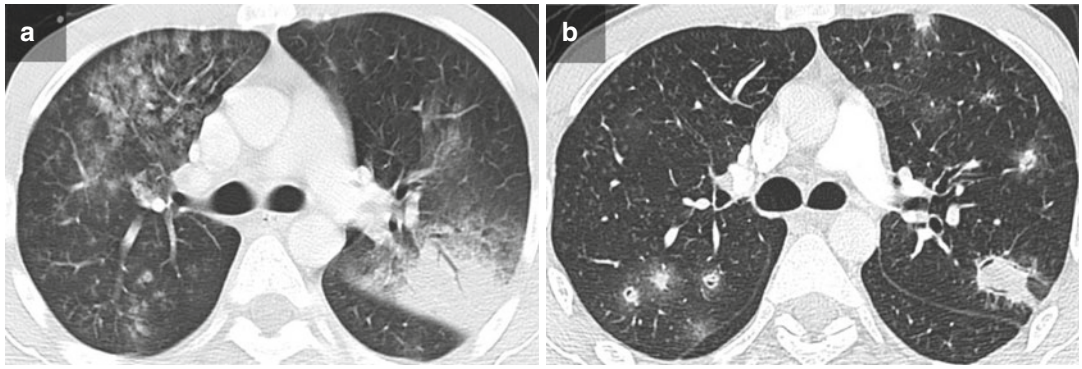

Fig. 42 Invasive aspergillosis in a 27-year-old woman with acute myeloid leukemia. Baseline CT (**a**) performed in a context of febrile agranulocytosis (**a**) with 5 mm-thick axial sections shows alveolar consolidation of the posterior segment of the upper part of the LUL with peripheral ground-glass opacity. Bronchiolo-alveolar nodules with ill borders are also seen in the RUL. On CT performed 3 weeks after (**b**), during bone marrow recovery, multiple nodules with air-crescent sign were seen, this finding suggesting a rather late stage of angioinvasive aspergillosis. Note the somewhat atypical presence of peripheral ground glass at this late stage of the disease

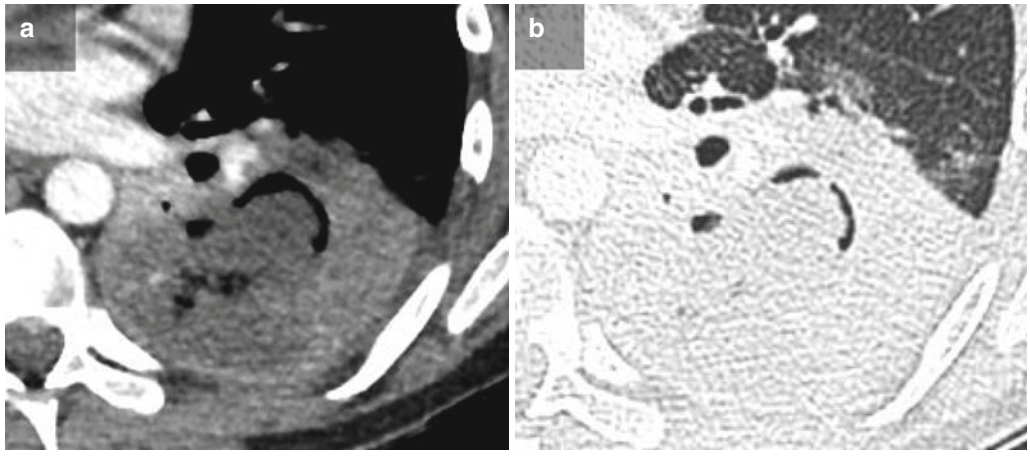

Fig. 43 Necrotizing pneumonia in a context of mucormycosis (same patient as in Fig. 13) presenting with hemoptysis 2 weeks after initial diagnosis despite adequate treatment. The retraction of the central necrotic mass of the LLL creates an air-crescent sign visible on mediastinal (**a**) and lung (**b**) windows. It had occurred at the same time as the pulmonary artery involvement

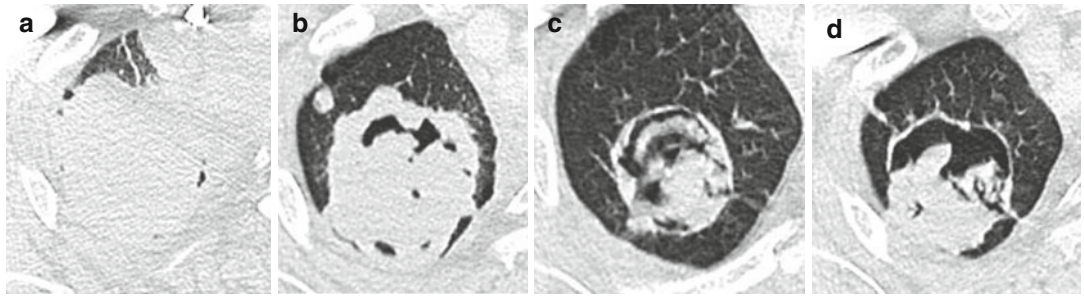

Fig. 44 Air-crescent sign caused by an invasive epidermoid carcinoma stage IIIb treated by radiochemotherapy that progressively cavitated. Axial image at baseline CT (**a**), 3 weeks (**b**) and two consecutive axial CT images performed 3 months (**c**, **d**) after beginning of the treatment. The necrotic tumor appears progressively as a pseudo-aspergilloma with an air-crescent sign

Numerous noninfectious disorders may also manifest with pneumatoceles/cysts, including cavitary metastases.

3.4.6 Meniscus, Cumbo, and Water Lily Signs

Meniscus, cumbo, and water lily signs are related to air dissecting the different layers of an echinococcal cyst secondary to bronchial erosion (Walker et al. 2014).

While a pericystic emphysema or meniscus sign refers to air between the outer pericyst and ectocyst, the cumbo sign is related to air penetrating the endocyst with an air-fluid level capped with air between pericyst and endocyst. The water lily sign relates to the ruptured hydatid cyst with the endocyst membrane floating on surface fluid (Walker et al. 2014).

3.5 Associated Abnormalities

3.5.1 Mediastinal and Hilar Abnormalities

- The most common mediastinal and hilar abnormality is *lymphadenopathy* (Fig. 45). Right paratracheal, hilar, and subcarinal regions and/or hilar lymph node enlargement with associated homolateral small focal infiltrate or parenchymal consolidation, which is commonly sublobar and subpleural in location in the middle lobe, basal segments of lower lobes, and anterior segments of upper lobes, is the usual hallmark of primary TB (Beigelman et al. 2000). Necrotic components with peripheral rim enhancement (rim sign) mainly suggest tuberculosis, but they can also correspond to fungal infection, atypical mycobacteria, histoplasmosis, metastases (Fig. 46) from head/neck and testicular malignancy, and lymphoma (Bhalla et al. 2015). Bronchonodal fistula can be observed as a complication of active pulmonary TB with TB lymphadenitis especially in the elderly. The fistulas usually involve the right lobar bronchus and the main bronchus on the left side (Park et al. 2015).
- A circumferential thickening of the *esophagus* may be related to a *cytomegalovirus* (CMV) infection, esophagitis being the second most common gastrointestinal manifestation of this organism after colitis (Wang et al. 2015), or *Candida* (Kuyumcu 2015) infection in immunocompromised patients.

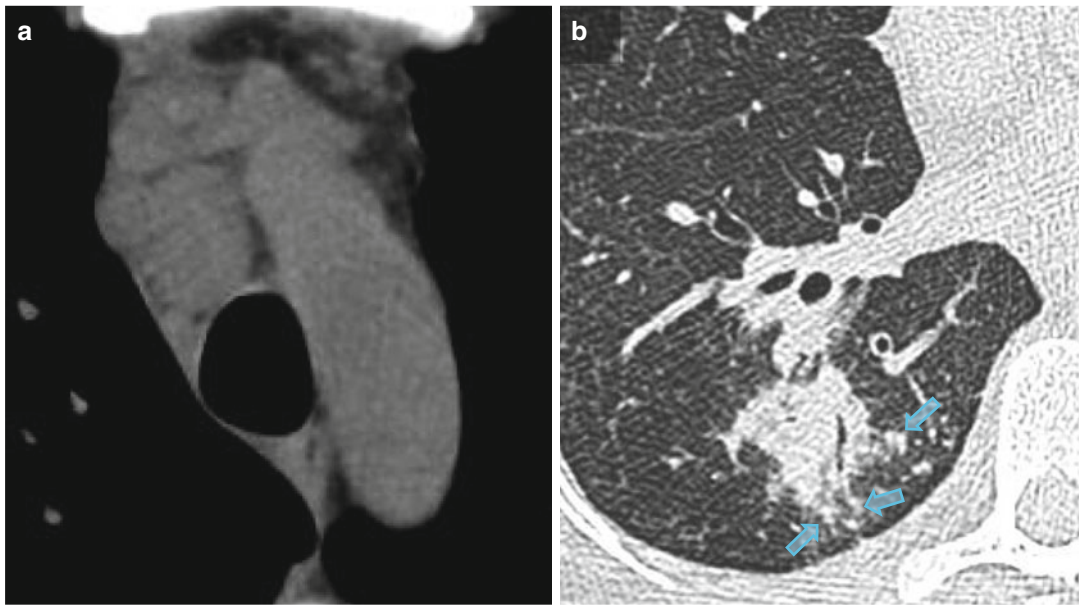

Fig. 45 Tuberculosis in a patient with a history of ulcerous colitis under anti-TNF treatment and lung graft for panlobular emphysema related to α1-antitrypsin deficiency. Axial sections in mediastinal (**a**) and lung (**b**) windows show an enlarged right paratracheal lymph node associated with a homolateral alveolar consolidation of the RLL, hallmarks of primary TB. Note the peripheral centrilobular nodules (*arrows*)

- In case of a circumferential thickening of the *trachea* or main bronchi occurring in the same context, the possibility of invasive aspergillosis of the respiratory tract should always be considered (Fig. 47) with the specific risk of tracheal rupture. Acute tuberculous tracheobronchial involvement may also be seen with circumferential narrowing associated with smooth or irregular wall thickening (Bhalla et al. 2015). Sequelar fibrotic bronchostenosis predominating on the left main bronchus and post-obstructive bronchiectasis may occur in this setting (Bhalla et al. 2015).
- Acute *infectious mediastinitis* may rarely be observed. It appears as increased soft tissue attenuation of mediastinal fat with fluid collections, air bubbles, air-fluid levels, and pneumomediastinum, with pericardial/pleural effusion. Regarding chronic or fibrosing mediastinitis, especially related to tuberculosis and fungal infections, including histoplasmosis, aspergillosis, mucormycosis, cryptococcosis, and blastomycosis, CT may display focal or diffuse involvement with calcifications as well as stenosis/obstruction of the vessels, airways, or esophagus (Akman et al. 2004).

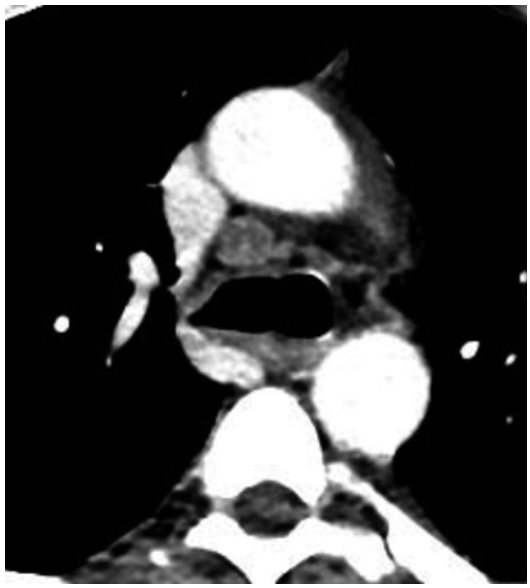

Fig. 46 Right paratracheal lymph node metastasis with necrosis and parietal enhancement in a patient treated by chemotherapy and immunotherapy in a context of a poorly differentiated carcinoma with hepatic and bone metastases

3.5.2 Pleural Abnormalities

- *Pleural effusions*, sometimes loculated, are encountered in 20–60 % of acute bacterial pneumonias. Most of the parapneumonic effusions without pleural thickening resolve under adequate medical treatment.

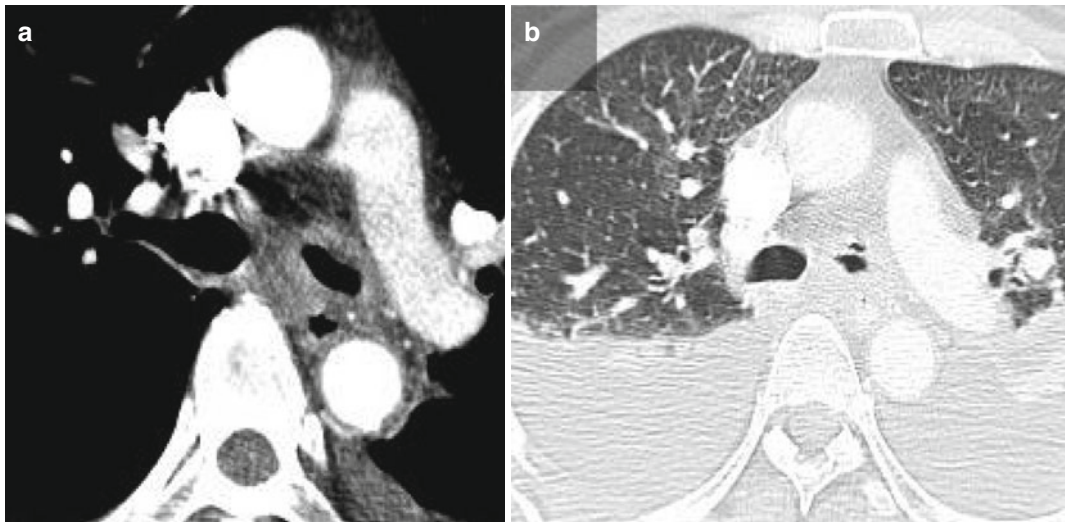

Fig. 47 Airway aspergillosis in a 74-year-old woman with lymphoma of the marginal zone complaining of cough and fever. A circumferential peribronchial thickening around the mainstem left bronchus is seen on the axial CT image with mediastinal window (**a**). Two weeks later, a worsening of the stenosis with a wall fistula is observed on the axial image with the lung window (**b**). Note the presence of a bilateral pleural effusion

- *Empyema*, which occurs in less than 5% of pulmonary infections, typically displays obtuse angles along its interface with adjacent pleura. It appears as a smooth and thin enhancement of the visceral and parietal pleura that surrounds the fluid collection and that is referred as the split pleura sign (Walker et al. 2014) (Figs. 10 and 11). It is commonly associated with a hyperattenuation of the extra-pleural fat. The pathogens traditionally involved in empyema are *S. pneumoniae*, *Streptococcus pyogenes*, and *S. aureus*. The same findings may be seen in case of TB.
- In this setting, an air-fluid level suggests a *bronchopleural fistula* (Walker et al. 2014), which is a sinus tract between a bronchus and the pleural space that most often results from a necrotizing pneumonia. CT features of bronchopleural fistula include an intrapleural airspace of various sizes, a new or changed air-fluid level, and, possibly, a fistulous communication, which may be become visible after the use of mIP post-processing. The air-fluid level within the pleura usually exhibits a length disparity when comparing posterior and lateral chest radiographs or between coronal and sagittal reformats unlike an air-fluid level associated with a pulmonary abscess typically displaying a spherical shape (Walker et al. 2014).

3.5.3 Other Features

- *Mycotic aneurysms* of pulmonary vessels may be observed in case of hemoptysis and a context of invasive fungal infections (Georgiadou et al. 2011) or tuberculosis (Fig. 12).
- *Spondylodiscitis* and/or an intramuscular *cold abscess* firstly suggests tuberculosis. A wavy periosteal reaction highly suggests thoracic actinomycosis.
- Concomitant small hypodense *lesions in the liver and/or spleen* may suggest pyogenic abscesses or fungal infections, in particular candidiasis.
- A worsening of CT findings may be encountered in case of "immune reconstitution inflammatory syndrome" *(IRIS)*. This syndrome is related to paradoxical worsening of preexisting infectious processes such as mycobacterial, viral, and *Pneumocystis jirovecii* infection following the initiation of highly active antiretroviral therapy (HAART) in HIV-infected individuals, a low CD4+ T-cell count being a major risk factor (Huis in 't Veld et al. 2012). IRIS syndrome may also be encountered in HIV-negative patients in conditions such as following corticosteroid withdrawal, discontinuation of antitumor necrosis factor-alpha therapy or recovery of neutropenia after cytotoxic chemotherapy, and engraftment of stem cell transplantation. It may be then observed in case of aspergillosis, candidiasis, and viral pneumonitis (Cheng et al. 2000).

3.6 Sequelae

Fibro-parenchymal lesions with bronchovascular distortion and bronchiectasis, thin-walled cavities, emphysema, and fibro-atelectatic bands firstly suggest prior tuberculosis with scarring (Fig. 48). Calcified mediastinal/hilar lymph nodes (Fig. 49), well-defined nodules, and pleural thickening with or without calcification (Fig. 50) are also common imaging features of healed TB. Tuberculomas and small calcified lung nodules suggest likewise prior TB infection (Bhalla et al. 2015). Calcified nodules may also be seen as sequelae of histoplasmosis or varicella infection (Chou et al. 2015) but also in other conditions like amyloidosis or metastasis, in particular from osteogenic sarcoma or medullary carcinoma of the thyroid.

Calcified peribronchial lymph nodes can erode into adjacent bronchi or cause distortion of the latter and can generate a broncholithiasis (Bhalla et al. 2015).

In conclusion, the recognition of the main CT pattern in association with the knowledge of the underlying disorders and the clinical context permits to strongly narrow the differential diagnosis. The application of a good technique is crucial for patients' management. In all cases, a multidisciplinary approach ensures the best outcome for the patient.

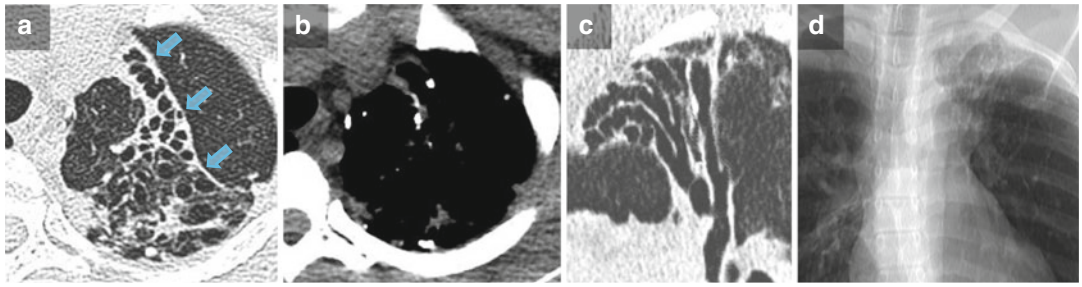

Fig. 48 Sequelae of TB in a 35-year-old woman originating from Cameroun. Axial section in parenchymal (**a**) and mediastinal windows (**b**) at the level of the upper lobes showing cicatricial collapsus of the upper part of LUL well delineated by a small accessory fissure (*arrows*) with bronchovascular distortion, bronchiectasis, thin-walled cavities, and calcified nodules. The 3 mm-thick mIP oblique reformat (**c**) allows for an overall assessment of the bronchiectasis. The coronal 150 mm-thick AIP reformat (**d**) shows the upper retraction of the left hilum

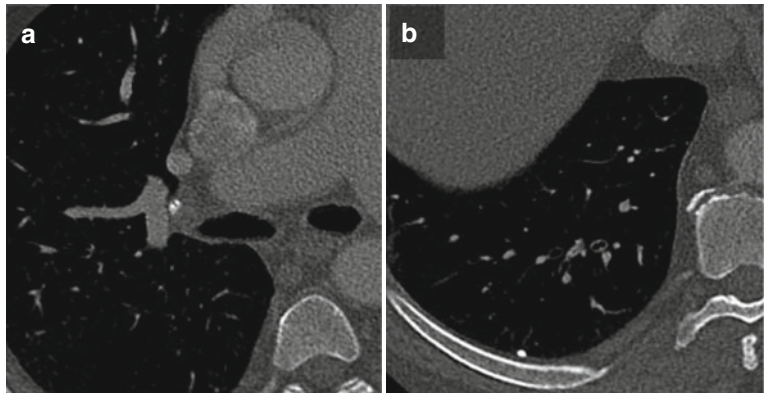

Fig. 49 Ranke complex related to scars from a previous primary TB. Axial section with the bone window at the level of the right hilum (**a**) and of the RLL (**b**) show a calcified hilar node and a calcified parenchymal nodule, respectively

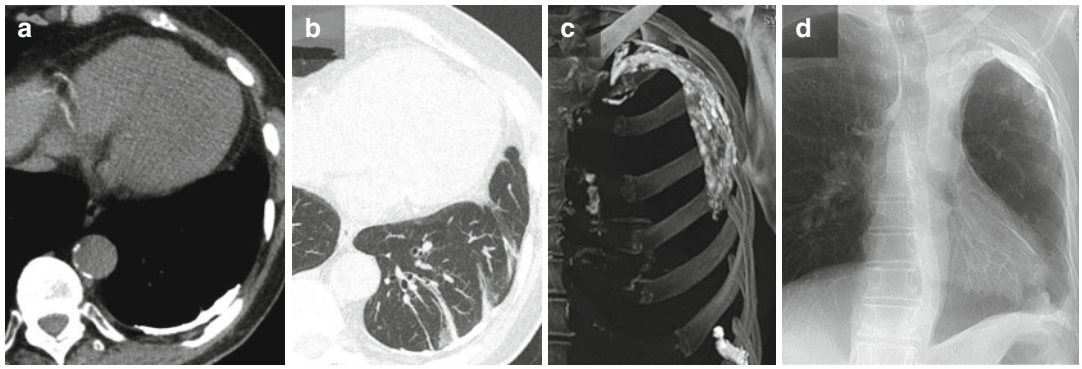

Fig. 50 A 77-year-old man with a calcified fibrothorax as a sequelae of a previous TB. Axial section in mediastinal (**a**) and lung (**b**) windows show a pleural calcification with parenchymatous bands converging toward the latter and related to fibrosis of the visceral pleura. A 70 mm-thick MIP coronal reformat in bone window (**c**) shows the upper predominance of this fibrothorax. A 180 mm-thick AIP reformat (**d**) reproducing the chest X-ray appearance shows the retraction of the left hemithorax and the blunting of the costophrenic angle, a classical finding in this setting

Acknowledgment Thanks to Pr Laurent Nicod, Pr John-David Aubert, Dr Frederic Tissot, Dr Francesco Doentz and Dr Khalid Alfudhili for their help.

References

Akman C, Kantarci F, Cetinkaya S (2004) Imaging in mediastinitis: a systematic review based on aetiology. Clin Radiol 59:573–585

Althoff Souza C, Müller NL, Marchiori E et al (2006) Pulmonary invasive aspergillosis and candidiasis in immunocompromised patients: a comparative study of the high-resolution CT findings. J Thorac Imaging 21(3):184–189

American Thoracic Society/Infectious Diseases Society of America (2005) Guidelines for the management of adults with hospital-acquired, ventilator-associated, and healthcare-associated pneumonia. Am J Respir Crit Care Med 171(4):388–416

Bankier AA, Tack D (2010) Dose reduction strategies for thoracic multidetector computed tomography background, current issues, and recommendations. J Thorac Imaging 25:278–288

Barnes PD, Marr KA (2007) Risks, diagnosis and outcomes of invasive fungal infections in haematopoietic stem cell transplant recipients. Br J Haematol 139:519–531

Beigelman C, Sellami D, Brauner M (2000) CT of parenchymal and bronchial tuberculosis. Eur Radiol 10: 699–709

Beigelman-Aubry C, Hill C, Guibal A et al (2005) Multidetector row CT and postprocessing techniques in the assessment of diffuse lung disease. Radiographics 25(6):1639–1652

Beigelman-Aubry C, Godet C, Caumes E (2012) Lung infections: the radiologist's perspective. Diagn Interv Imaging 93:431–440

Bhalla M, McLoud T (1998) Pulmonary infections in the normal host in thoracic radiology. In: Mc Loud T (ed) The requisistes. James H. Thrall Mosby: Philadelphia; pp 91–133

Bhalla AS, Goyal A, Guleria R (2015) Chest tuberculosis: radiological review and imaging recommendations. In J Radiol Imag 25(3):213–225

Caillot D, Couallier JF, Bernard A et al (2001) Increasing volume and changing characteristics of invasive pulmonary aspergillosis on sequential thoracic computed tomography scans in patients with neutropenia. J Clin Oncol 19:253–259

Chang CH, Ruan SY, Li CC, Yu CJ (2013) Non-human immunodeficiency virus Pneumocystis jirovecii pneumonia. Respirology 18(1):191–192

Cheng VCC, Yuen KY, Chan W et al (2000) Immunorestitution disease involving the innate and adaptive response. Clin Infect Dis 30:882–892

Chou CC, Shen T-C, Tu C-Y et al (2015) Calcified pulmonary nodules. Eur J Intern Med 26:e27–e28

Christe A, Lin MC, Yen AC et al (2012) CT patterns of fungal pulmonary infections of the lung: comparison of standard-dose and simulated low-dose CT. Eur J Radiol 8:2860–2866

De Marie S (2000) New developments in the diagnosis and management of invasive fungal infections. Haematologica 85:88–93

Dodd JD, Souza CA, Müller NL (2006) High-resolution MDCT of pulmonary septic embolism: evaluation of the feeding vessel sign. AJR Am J Roentgenol 187(3): 623–629

Festic E, Gajic O, Limper AH, Aksamit TR (2005) Acute respiratory failure due to pneumocystis pneumonia in patients without human immunodeficiency virus infection: outcome and associated features. Chest 128(2): 573–579

Francis JS, Doherty MC, Lopatin U et al (2005) Severe community-onset pneumonia in healthy adults caused by methicillin-resistant Staphylococcus aureus carrying the Panton-Valentine leukocidin genes. Clin Infect Dis 40(1):100–107

Franquet T (2006) High-resolution computed tomography (HRCT) of lung infections in non-AIDS immunocompromised patients. Eur Radiol 16:707–718

Franquet T (2008) Pulmonary infection in adults. In: Adam A, Dixon AK, Gillard JH, Shaefer-Prokop CM (eds) Diagnostic radiology grainger & Allison's Churchill Livingsrone. Elsevier: Edinburgh, London, New York; p 246–266

Franquet T (2011) Imaging of pulmonary viral pneumonia. Radiology 260(1):18–39

Franquet T, Müller NL, Giménez A, Martínez S, Madrid M, Domingo P (2003) Infectious pulmonary nodules in immunocompromised patients: usefulness of computed tomography in predicting their etiology. J Comput Assist Tomogr 27(4):461–468

Georgiadou SP, Sipsas NV, Marom EM et al (2011) The diagnostic value of halo and reversed halo signs for invasive mold infections in compromised hosts. Clin Infect Dis 52(9):1144–1155

Greene RE, Schlamm HT, Oestmann JW et al (2007) Imaging findings in acute invasive pulmonary aspergillosis: clinical significance of the halo sign. Clin Infect Dis 44(3):373–379

Hansell DM, Bankier AA, MacMahon H et al (2008) Fleischner Society: glossary of terms for thoracic imaging. Radiology 246:697–722

Herold CJ, Sailer JG (2004) Community-acquired and nosocomial pneumonia. Eur Radiol 14(Suppl 3):E2–E20

Heussel CP, Kauczor HU, Heussel GE et al (1999) Pneumonia in febrile neutropenic patients and in bone marrow and blood stem-cell transplant recipients: use of high-resolution computed tomography. J Clin Oncol 17:796–805

Huis in 't Veld D, Sun HY, Hung CC (2012) The immune reconstitution inflammatory syndrome related to HIV co-infections: a review. Eur J Clin Microbiol Infect Dis 31:919–927

Jones RN (2010) Microbial etiologies of hospital-acquired bacterial pneumonia and ventilator-associated bacterial pneumonia. Clin Infect Dis 51(Suppl 1):S81–S87

Kang EY, Patz EF Jr, Müller NL (1996) Cytomegalovirus pneumonia in transplant patients: CT findings. J Comput Assist Tomogr 20:295–299

Kim HJ, Park SY, Lee HY et al (2014) Ultra-low-dose chest CT in patients with neutropenic fever and hematologic malignancy: image quality and its diagnostic performance. Cancer Res Treat 46(4):393–402

Kjeldsberg KM, Oh K, Murray KA et al (2002) Radiographic approach to multifocal consolidation. Semin Ultrasound CT MR 23:288–301

Kuyumcu S (2015) Candida esophagitis mimicking esophageal malignancy on 18FDG PET/CT. Turk J Gastroenterol 26:63–64

Logan PM, Primack SL, Miller RR, Müller NL (1994) Invasive aspergillosis of the airways: radiographic, CT, and pathologic findings. Radiology 193(2):383–388

McGuinness G, Scholes JV, Garay SM et al (1994) Cytomegalovirus pneumonitis: spectrum of parenchymal CT findings with pathologic correlation in 21 AIDS patients. Radiology 192(2):451–459

Morikawa K, Okada F, Ando Y et al (2012) Methicillin-resistant Staphylococcus aureus and methicillin-susceptible S. aureus pneumonia: comparison of clinical and thin-section CT findings. Br J Radiol 85:e168–e175

Muller N (2003) Pulmonary infections in diseases of the lung. In: Muller N (ed) Radiologic and pathologic correlations. Lippincott Williams & Wilkins: Baltimore, Philadelphia; pp 17–75

Niedemann MS (2015) Community-Acquired Pneumonia. Ann Intern Med 163(7):ITC1

Oh YW, Effmann EL, Godwin JD (2000) Pulmonary infections in immunocompromised hosts: the importance of correlating the conventional radiologic appearance with the clinical setting. Radiology 217: 647–656

Park SH, Jeon KN, Park MY et al (2015) Tuberculous bronchonodal fistula in adult patients: CT findings. Jpn J Radiol 33:360–365

Schulze M, Vogel W, Spira D et al (2012) Reduced perfusion in pulmonary infiltrates of high-risk hematologic patients is a possible discriminator of pulmonary angioinvasive mycosis: a pilot volume perfusion computed tomography (VPCT) study. Acad Radiol 19(7):842–850

Stigl WI, Marrie TJ (2013) Severe community-acquired pneumonia. Crit Care Clini 29:563–601

Syrjälä H, Broas M, Suramo I, Ojala A, Lähde S (1998) High-resolution computed tomography for the diagnosis of community acquired pneumonia. Clin Infect Dis 27:358–363

Tanaka N, Matsumoto T, Kuramitsu T et al (1996) High resolution CT findings in community-acquired pneumonia. J Comput Assist Tomogr 20:600–608

Tasaka S, Tokuda H (2012) Pneumocystis jirovecii pneumonia in non-HIV-infected patients in the era of novel immunosuppressive therapies. J Infect Chemother 18(6):793–806

Thomas CF Jr, Limper AH (2004) Pneumocystis pneumonia. N Engl J Med 350(24):2487–2498

Wahba H, Truong MT, Lei X, Kontoyiannis DP, Marom EM (2008) Reversed halo sign in invasive pulmonary fungal infections. Clin Infect Dis 46: 1733–1737

Walker CM, Abbott GF, Greene RE (2014) Imaging pulmonary infection: classic signs and patterns. AJR 202:479–492

Wang HW, Kuo CJ, Lin W-R et al (2015) The clinical characteristics and manifestations of cytomegalovirus esophagitis. Dis Esophagus. pp 1–8. doi:10.1111/dote.12340